The Thesis Committee for Adam Drescher
Certifies that this is the approved version of the following thesis:

Characterization of $LaBr_3$:Ce Detectors in a Gamma-Gamma Coincidence Configuration

APPROVED BY
SUPERVISING COMMITTEE:

Supervisor:

Sheldon Landsberger

Derek Haas

Characterization of $LaBr_3$:Ce Detectors in a Gamma-Gamma Coincidence Configuration

by

Adam Drescher, B.S. Physics

Thesis

Presented to the Faculty of the Graduate School of

The University of Texas at Austin

in Partial Fulfillment

of the Requirements

for the Degree of

Master of Science in Engineering

The University of Texas at Austin

May 2017

Dedication

I dedicate this work to my parents, Bill and Carol Drescher, for always encouraging me to do my best work.

Acknowledgements

I would like to thank Dr. Sheldon Landsberger for his significant investments of time and effort in helping me achieve success with my research and academic career in gamma spectroscopy. His insights and wisdom have been invaluable resources to me. I would also like to thank Derek Haas, who provided valuable feedback during the final steps of the preparation of this thesis.

This work has been financially supported by a fellowship through the Consortium for Nonproliferation Enabling Capabilities.

Abstract

Characterization of $LaBr_3$:Ce Detectors in a Gamma-Gamma Coincidence Configuration

Adam William Drescher, M.S.E.

The University of Texas at Austin, 2017

Supervisor: Sheldon Landsberger

A radiation detection system consisting of two cerium doped lanthanum bromide ($LaBr_3$:Ce) scintillation detectors in a gamma-gamma coincidence configuration has been used to demonstrate the advantages that coincident detection provides relative to a single detector, and the advantages that $LaBr_3$:Ce detectors provide relative to high-purity germanium (HPGe) detectors. Measurements have been made in both single and coincident detector configurations with both detector technologies to quantify the performance of each detector configuration permutation. Timing performance and optimization of single and coincident systems have been performed for both detector types. The efficiency and energy resolution of $LaBr_3$:Ce detectors have been determined and compared to both HPGe detectors and MCNP simulations. Further MCNP simulations have validated single LaBr3:Ce detector response to a collection of radionuclides. Coincident gamma-ray pairs from the radionuclides ^{152}Eu and ^{133}Ba have been identified in a sample that is dominated by ^{137}Cs. Gamma-gamma coincidence successfully reduced the Compton continuum from

the large ^{137}Cs peak, revealed several coincident gamma energies characteristic of these nuclides, and improved the signal-to-noise ratio relative to single detector measurements. $LaBr_3$:Ce detectors performed at count rates multiple times higher than can be achieved with HPGe detectors. The standard background spectrum consisting of peaks associated with gamma-ray transitions within the $LaBr_3$:Ce crystal has also been significantly reduced. It is shown that $LaBr_3$:Ce detectors have the unique capability to perform gamma-gamma coincidence measurements in very high count rate scenarios, which can potentially benefit nuclear safeguards in situ measurements of spent nuclear fuel. As a scoping study for applications to spent nuclear fuel, a series of coincident measurements were made over the course of a month of fission products in irradiated uranium samples of varying enrichment levels.

Table of Contents

List of Tables

List of Figures

Chapter 1: Introduction

Gamma-ray spectrometry is a robust, nondestructive measurement technique for the quantification of radionuclides. However, there are many different variations in gamma-ray spectrometry, each of which have advantages under different measurement conditions. When performing a measurement with gamma-ray spectrometry, it is important to select a system that will provide the best performance under the expected measurement conditions. Parameters of gamma-ray spectrometry that can be altered to suit the detection requirements include: choice of detector (i.e. semiconductors vs scintillators), use of coincidence or anti-coincidence (Compton suppression) measurements, whether or not to employ list-mode data acquisition, etc. The present work will compare a few of the detector configuration options available, as well as introduce a presently under-studied detector configuration: coincident $LaBr_3$:Ce scintillation detectors.

This experiment will be put into a modern context by first conducting a review of existing detection system configurations, with both theoretical and application-based discussions. The operational principles, strengths, and weaknesses associated with each of these popular configurations will be discussed.

The proposed detection system will provide unique detection capabilities that are absent in the mainstream detection system configurations. This will be discussed on a theoretical basis, and then proven with experimental results.

The purpose of this work is therefore to present the capabilities of this new radiation detection system consisting of $LaBr_3$:Ce detectors in a coincidence configuration with benchmarks to existing and proven systems including a single $LaBr_3$:Ce detector, a single HPGe detector, coincident HPGe detectors, and MCNP simulations. Each of these four detector configurations will be subject to a battery of experiments which will quantify their absolute and relative performances with regards to efficiency, energy resolution, and peak to Compton ratios.

It is demonstrated that coincident $LaBr_3$:Ce detectors have the unique capability to perform gamma-gamma coincidence measurements in very high count rate scenarios. This will advance

the field of gamma-ray spectrometry by extending the capabilities of gamma-gamma coincidence measurement to situations involving high count rates, such as nuclear safeguards in situ measurements of spent nuclear fuel.

MOTIVATION

Characterization of spent and reprocessed nuclear fuel presents several challenges to conventional HPGe single detector gamma spectroscopy. Three challenges directly addressed using coincident $LaBr_3$:Ce detectors are 1) high count rates that result in significant dead time limiting the rate of data collection and reducing statistical precision; 2) gamma spectra containing a large, diverse range of fission products complicates peak identification due to interference and intense Compton scatter; 3) transportation of spent nuclear fuel is expensive and time-intensive due to regulatory and safety concerns. These challenges place emphasis on the need for a system with strong background suppression, the best achievable energy resolution, and portability. Simulated gamma-ray spectrum deconvolution performed using a 2.54 cm x 2.54 cm (1 in. x 1 in.) cerium doped lanthanum bromide detector was used to nondestructively determine the burn-up of spent nuclear fuel from the Advanced Test Reactor (ATR) on-site (Navarro, Ring, & Nigg, 2014).

Cerium doped lanthanum bromide ($LaBr_3$:Ce) is an excellent detector choice to potentially meet all of the above mentioned criteria. The efficiency of $LaBr_3$:Ce detectors is superior to that of thallium doped sodium-iodide detectors (Saint Gobain, 2009). $LaBr_3$:Ce detectors have been shown to be 1.2-1.65 times more efficient than NaI:Tl detectors above 350 keV, for 3.8 cm x 3.8 cm (1.5 in. x 1.5 in.) detectors (Ciupek, Jednoróg, Fujak, & Szewczak, 2014). The energy resolution of $LaBr_3$:Ce detectors is superior to that of NaI:Tl detectors (Saint Gobain, 2009). $LaBr_3$:Ce detectors have an energy resolution of 2.5-3% at the 662 keV gamma line of ^{137}Cs compared to 6-7% for NaI:Tl detectors (Ciupek et al., 2014). These advantages over NaI:Tl detectors have been demonstrated in an experiment which shows that $LaBr_3$:Ce detectors find more distinguishable peaks than NaI:Tl detectors with a higher efficiency (Milbrath et al., 2007). The

lack of need for liquid nitrogen cooling also makes $LaBr_3$:Ce systems significantly more portable than HPGe. $LaBr_3$:Ce has been shown to be an excellent detector choice for high count rate scenarios, and is capable of performing well with count rates up to 500 kHz (Löher et al., 2012). In the past, MCNPX calculations have been utilized to verify that $LaBr_3$:Ce scintillators can accurately identify isotopes in a fuel element spectrum (Navarro et al., 2014). These results suggest that $LaBr_3$:Ce detectors will be useful in the characterization of spent nuclear fuel as well.

There are challenges associated with using $LaBr_3$:Ce detectors. First, $LaBr_3$:Ce is itself radioactive, due to natural abundances of lanthanum containing radioactive ^{138}La (Ciupek et al., 2014; Saint Gobain, 2009). ^{138}La accounts for 0.09% of all naturally occurring lanthanum and produces two gamma rays: a 788.7 keV gamma-ray from beta decay to ^{138}Ce, and a 1435.8 keV gamma ray from electron capture to ^{138}Ba. ^{138}La has a 1.02×10^{11} year half-life, and thus results in background count rates of 0.065 cps/cm^3 and 0.068 cps/cm^3 from its two photopeaks respectively.

These intrinsic photopeaks degrade the detection limits at and below these energies during typical single-channel spectrum collection (Saint Gobain, 2009). In principle, these background features could be subtracted from single-channel spectra. However, this would create additional statistical uncertainties in the remaining results. Therefore, the preferred method of background elimination in this work is gamma-gamma coincidence gating with multiple detectors. One advantage to this internal radioactivity is that it provides a means of self-calibration of energies up to nearly 3000 keV (using the random coincidence of two 1435.8 keV gamma rays). This advantage is particularly useful for autonomous portable systems that may not always have access to standard gamma sources in a typical laboratory setting, and is unique to $LaBr_3$:Ce (Xiang et al., 2013). It will also be shown that gamma-gamma coincidence methods are effective for eliminating the contributions from inherent radioactivity when self-calibration is not required.

A coincidence configuration of these detectors will be used for de-convolution of peaks and reduction of background, allowing for more precise characterization of complex spectra. Gamma-gamma coincidence has the advantage of virtually eliminating all background peaks that do not exist in coincidence with other peaks, significantly improving detection limits of useful

radionuclides (Horne & Landsberger, 2011; Yoho & Landsberger, 2015). The main disadvantage of this method is that it can only be applied to the detection of isotopes with coincident decay schemes. Other disadvantages that can be overcome through development of the technique are identification of particularly useful signatures and commercial software to analyze the resulting complicated spectra. By employing gamma-gamma coincidence, the background from the radioisotopes in the $LaBr_3$:Ce scintillator is eliminated, providing a means for improving detection limits.

Resulting from a lack of readily available spent nuclear fuel, experiments were performed on a superposition of radioactive sources representing a high count rate and complicated spectrum, thus artificially simulating the potential situation of spent nuclear fuel. Experiments were performed with a single $LaBr_3$:Ce detector, a single HPGe detector, coincident $LaBr_3$:Ce detectors, and coincident HPGe detectors. Count rates were varied from 20 to 400 kHz. Sources included 50 mCi of ^{137}Cs, and 10 μCi of ^{133}Ba and ^{152}Eu. This combination of configurations provides multi-variate comparators to benchmark the signal-to-noise performance of each detector type as a function of: number of detectors, input count rate, and energy. In the final portion of this work, the coincident $LaBr_3$:Ce detectors are subject to a difficult measurement: high activity irradiated uranium samples of varying initial enrichments. This will serve as a more realistic analog to a real-world nuclear safeguards application such as measurements of highly active spent nuclear fuel.

Chapter 2: Theory

GAMMA SPECTROSCOPY

Gamma-ray spectroscopy is a well-developed measurement technique for the nondestructive determination of radionuclide contents in a sample. It has the capability to determine the particular radionuclides present in a sample, as well as the activity or concentration within that sample. Determination of particular radionuclides relies on measurement of the full energy of gamma-rays emitted by the radionuclides. The particular energy of the emitted gamma-ray is a property of each radionuclide, and thus serves as an indicator of the presence of that radionuclide. Determination of the concentration of each radionuclide relies on measurement of the rate of emission of each gamma-ray energy. This section will discuss the physical interactions that must occur during gamma-ray spectroscopy.

INTERACTIONS OF GAMMA-RADIATION WITH MATTER

Detection of gamma radiation is possible due to the fundamental ways in which gamma-rays interact with matter. The primary ways in which gamma-rays interact with matter include: The Photoelectric Effect, Compton Scattering, and Pair Production. Material for this section is referenced from (Knoll, 2010).

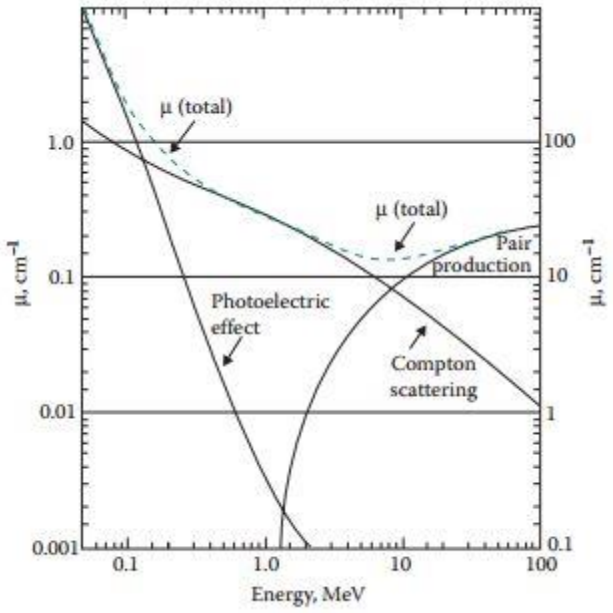

Figure 1: The relative interaction probabilities of photons in matter as a function of energy.

For low energy gamma-rays (typically energies less than 200 keV), the most likely interaction with matter is The Photoelectric Effect. This is the phenomenon in which a photon strikes an electron and deposits all of its energy in the electron. The photon is eliminated in this process, and the electron gains kinetic energy equal to the initial energy of the photon less the electron's binding energy to the atom in which it was initially contained. The electron is ejected from the atom and can then either interact further or escape, depending on the particular material and geometry in which it is contained. This effect is strongest in high Z materials due to the greater electron density.

Intermediate energy photons (typically energies ranging from 200 keV-1.022 MeV) primarily interact with matter via Compton Scattering. This is the phenomenon in which a photon strikes an electron and imparts only some of its energy to the electron. The photon and electron both survive this interaction, and continue on with a redistribution of the system's initial energy. The kinematic equation describing Compton Scattering, where hv and hv' are the photon energies

before and after the interaction respectively, m_e is the mass of the electron, c is the speed of light, and θ is the scattering angle of the photon with respect to its initial direction of travel, is:

$$h\nu' = \frac{h\nu}{1 + \frac{h\nu}{m_e c^2}(1 - \cos\theta)}$$

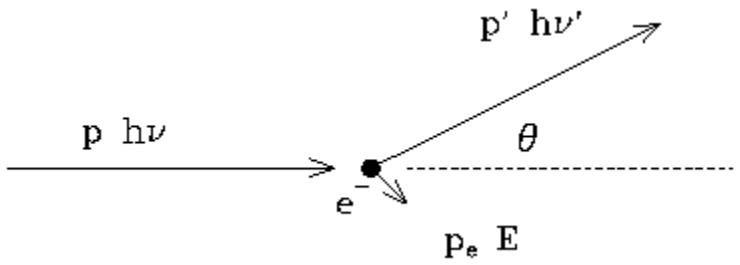

Figure 2: A schematic of Compton Scattering.

The scattered photons are created with an angular distribution which is described by the Klein-Nishina formula, where $\alpha = h\nu/m_0c^2$, which is given by:

$$\frac{d\sigma}{d\Omega} = Zr_0^2 \left(\frac{1}{1 + \alpha(1 - \cos\theta)}\right)^2 \left(\frac{1 + \cos^2\theta}{2}\right)\left(1 + \frac{\alpha^2(1 - \cos\theta)^2}{(1 + \cos^2\theta)[1 + \alpha(1 - \cos\theta)]}\right)$$

where $\frac{d\sigma}{d\Omega}$ is the differential scattering cross section, Z is the atomic number for the scattering nucleus, r_0 is the classical electron radius, and θ is the scattering angle.

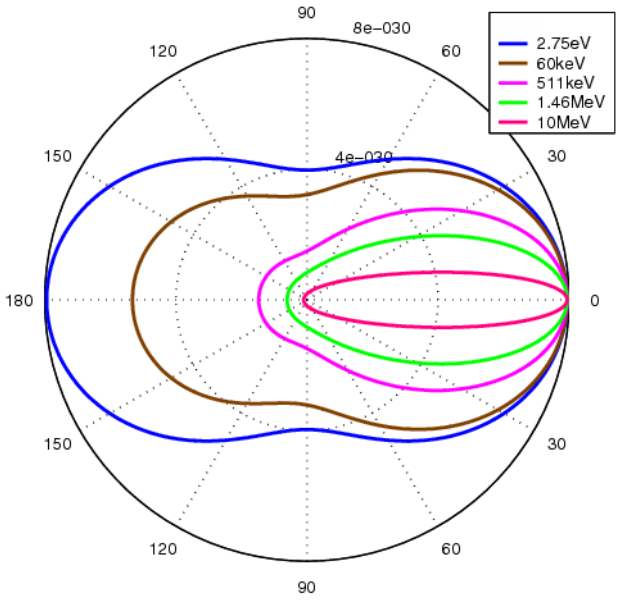

Figure 3: A plot of the angular distribution of Compton Scattered photons for a variety of initial photon energies.

High energy photons primarily interact with matter via Pair Production. In the presence of a strong electric field, such as near an atomic nucleus, photons with energies of at least 1.022 MeV will spontaneously dissociate into an electron-positron pair. Due to the conversion of energy into matter, this is a threshold interaction that requires the initial photon to have at least as much energy as the mass of the created electron-positron pair: 1.022 MeV. Any additional photon energy above this threshold is distributed equally between the electron and positron as kinetic energy to conserve both energy and momentum. The electron may interact in the material or escape, depending on the particular material and geometry. The positron will slow as it deposits energy in the medium and quickly encounter an electron. This electron-positron pair will annihilate and produce two gamma-rays of 511 keV. These gamma-rays can then undergo further interactions such as Compton Scattering.

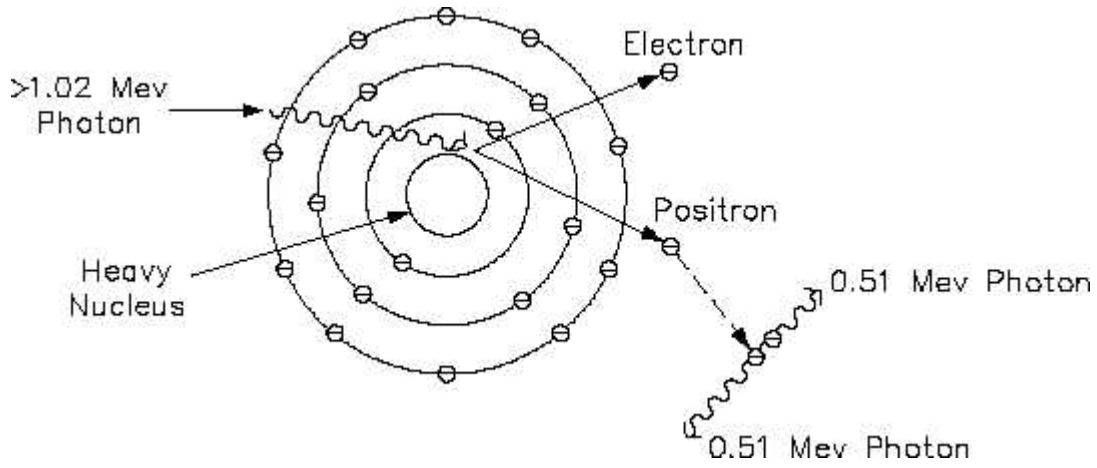

Figure 4: A schematic of pair production, including the eventual annihilation of the positron with a nearby electron.

GAMMA-GAMMA COINCIDENCE SPECTROSCOPY

Gamma-gamma coincidence spectroscopy is a variation on typical single detector gamma-ray spectroscopy which incorporates a second detector and timing logic to produce a multidimensional spectrum. A gamma-ray interaction event that occurs in one of the two detectors will only be placed in the resulting coincidence spectrum if it occurs simultaneously (within a user specified timing window) with a separate event in the other detector. The resulting gamma-ray spectrum, rather than being a histogram of energy bins on the x-axis and counts/bin on the y-axis, as in single detector gamma-ray spectroscopy, is a two dimensional "heatmap" in which the x- and y-axes both correspond to energy bins for each of the two detectors, and the grid contained by these axes is populated with coincidence events, the coordinates of which correspond to the two energies simultaneously deposited in each detector. The advantages of performing gamma-gamma coincidence measurements include:

- Strong suppression of background radiation and interferences resulting from decay of noncoincident-emitting radionuclides in the sample, which increases detection limits of coincidence-emitting radionuclides by several orders of magnitude

- Addition of timing information. A peak in a gamma-gamma coincidence spectrum contains two energy levels. If both energy levels of that peak are shown to correspond to the decay scheme of a particular radionuclide, it can be unambiguously identified.

One of the most important calibration parameters of a gamma-gamma coincidence system is the coincidence timing window. This is the duration of time during which any events that occur can be considered simultaneous, and thus incorporated into the coincidence heatmap. This window is typically on the order of tens to hundreds of nanoseconds, and must be optimized for each coincidence detection system. The size of the coincidence timing window is also highly dependent on the type of detector utilized. Other considerations include the possibility of a timing offset between the two detectors, which could result from different cable lengths, crystal sizes, or models of back-end electronics. Most coincidence analysis systems therefore include a timing offset that can be applied to correct for any timing differences that might be present in the system.

It is useful to discuss a few of the features that will typically appear in a gamma-gamma coincidence heatmap. These include true full-energy coincidence events, full-energy/Compton Scattering coincidence events, and 180 degree Compton Scattering events. For reference, an example coincidence heatmap is shown in the figure below.

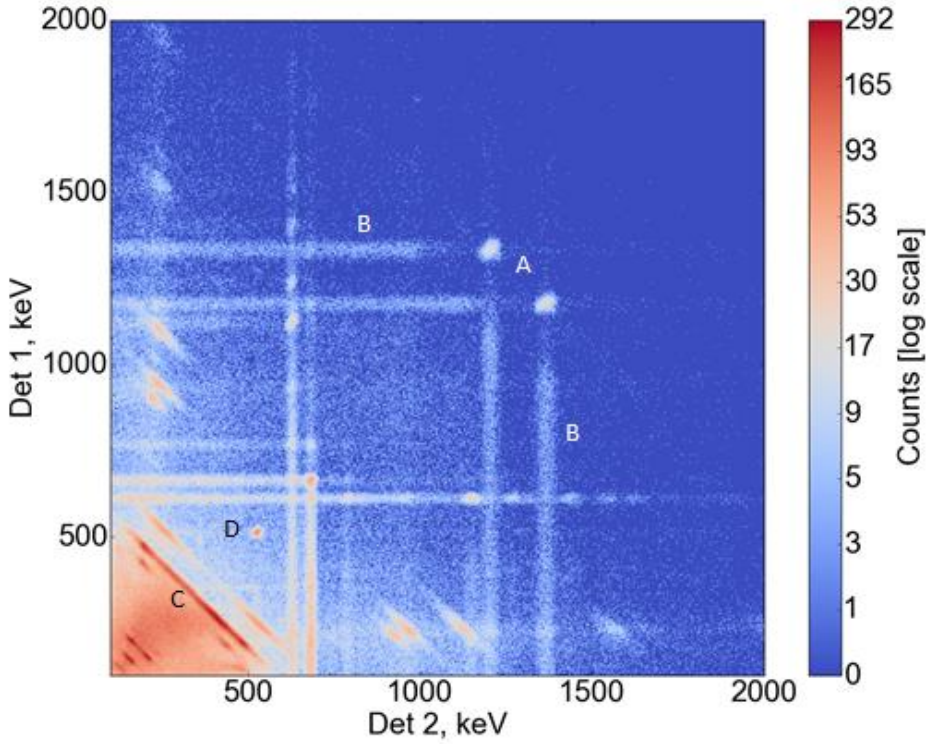

Figure 5: An example gamma-gamma coincidence heatmap. A) Two true full energy deposition coincidence events. B) A true coincidence with one full energy deposition and one Compton Scatter. C) 180 degree Compton Scattering events that hit both detectors. D) Positron annihilation peak.

One of the most prominent features of this figure are the two white dots located at energy coordinates (1173, 1332) and (1332, 1173). These two features represent true full energy deposition coincidence events between the two gamma-rays emitted by ^{60}Co at those same energies. Note the symmetry of these, and all other features of the coincidence heatmap about the diagonal line of equal detector energies. It makes intuitive sense that any coincidence event can occur with events A and B in detectors 1 and 2, or in detectors 2 and 1, respectively, and with equal probabilities.

Horizontal and vertical streaks are also seen, shooting off of these two dots. These features are true coincidence in which one of the gamma-rays Compton Scatters and only partially deposits energy in one detector, while the other gamma-ray fully deposits its energy in the other detector.

These vertical and horizontal lines are thus always seen in a coincidence heatmap stemming off of any gamma-ray coincidence energy pairs in the spectrumThese streaks are one of two types of Compton Continuums that manifest in any coincidence heatmap.

The next prominent feature that appears in all coincidence spectra are the diagonal streaks that appear in many locations throughout this spectrum. This is the other type of Compton Continuum present in any coincidence heatmap. These represent 180 degree Compton Scattering events, in which a gamma-ray deposits some of its energy in one detector, is scattered by 180 degrees, and deposits the rest of its energy in the opposite detector. The intensity of this Compton Scattering streak depends only on the intensity of the full energy gamma-ray to which it corresponds. Thus, the coordinates of any location on one of these streaks will sum to the full energy of an intense gamma-ray energy line in the single detector spectrum.

One more interesting aspect of this spectrum is the lone coincidence peak at roughly coordinates (500, 500). This is one of the only coincidence peaks in the spectrum that lacks the horizontal and vertical elements discussed earlier.. This coincidence peak is the (511 keV, 511 keV) annihilation peak caused by positrons and electrons annihilating and creating two 511 keV photons travelling in opposite directions. Annihilation events typically occur when the electron-positron pair have near zero kinetic energy. At this low energy, Compton Scattering is unlikely, and therefore there are no horizontal or diagonal streaks stemming off of this coincidence point. By the requirements of simultaneous conservation of energy and momentum, these 511 keV gamma-rays are always emitted in coincidence, and always travel in directly opposite directions. The combination of these factors makes it quite a strong coincidence peak.

SEMICONDUCTORS: HIGH-PURITY GERMANIUM

A gamma radiation detector is a material with favorable properties for the detection of gamma radiation. Favorable properties for gamma radiation detection include: the ability to generate a signal that is proportional to the incident gamma-ray energy, high gamma-radiation

absorption coefficient, good energy resolution, and stability over a variety of temperatures and settings. Material for this section is referenced from (Gilmore, 2008). Semiconductors are among the most popular detector technology of choice for a variety of gamma-spectroscopy applications. Here, the operational principles, advantages, and disadvantages of semiconductor detectors will be reviewed.

The operational principles of semiconductor detectors are based on the band structure of solids. In all materials, electrons exist within occupied bands or shells of the atoms. The highest energy electron shell is dubbed the valence band. Above the valence band, there is sometimes a band gap, above which there is a conduction band. Solid matter can then be distinguished into three categories based on the size of the band gap between the valence band and the conduction band. An electrical insulator is a material with a band gap of roughly 10 eV. On the other end, a conductor has no band gap. In this scenario, electrons can freely move between the valence band and the conduction band spontaneously. A semiconductor is an intermediate material between the two, with a small band gap of roughly 1 eV. However, at room temperatures, this band gap is small enough for electrons to spontaneously jump across the band gap and enter the conduction band from thermal excitations. Semiconductor detectors such as HPGe are therefore cooled with liquid nitrogen to about 77 K, which eliminates thermal excitations.

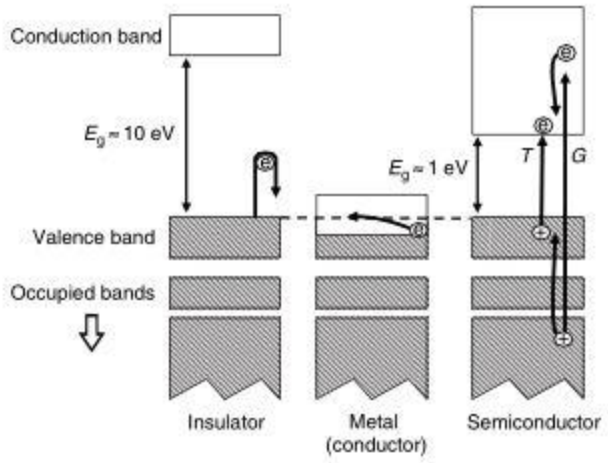

Figure 6: Schematic of the band structure of solids (Gilmore, 2008).

When a gamma-ray interacts with an electron in a semiconductor material, the electron is excited to the conduction band, and an electron-hole pair is produced. The electron-hole pair can interact with the material in a cascading manner, producing many electron hole pairs. The exact number of electron-hole pairs produced is proportional to the energy of the incident gamma-ray. The electrons are then collected by a high voltage applied across the detector material, and registered as a pulse in the back-end electronics.

Semiconductor detectors have the advantage of producing a large number of charge carriers for each gamma-ray interaction (compared to scintillation detectors). This results in the excellent energy resolution that is characteristic of semiconductor detectors such as high-purity germanium (HPGe). The fact that they are cooled by liquid nitrogen also ensures that they are stable under changing environmental and temperature conditions.

SCINTILLATORS: CERIUM-DOPED LANTHANUM BROMIDE

Scintillation detectors have fundamental operating principles that differ significantly from that of semiconductor detectors. Scintillation detectors are constructed with inorganic crystals such as sodium iodide (NaI) or lanthanum bromide ($LaBr_3$). However, these inorganic crystals are

electrical insulators. This means that they possess a large band gap between the valence band and conduction band. Electrons that are elevated to the conduction band by an incident gamma-ray will therefore de-excite with a high energy photon which will be readily absorbed by the surrounding material. This makes collection of the signal impossible. Therefore, activator impurities are introduced to the inorganic crystal to cause defects in the crystal lattice. For NaI, the activator is thallium (NaI:Tl), and for $LaBr_3$, the activator is cerium ($LaBr_3$:Ce). These activators have valence and conduction bands that are both within the valence band of the inorganic crystal material. This allows electron-hole pairs which are formed in the crystal to migrate to the activator impurities, and de-excite with a photon of visible wavelength. Because this photon is not of an energy level that matches the characteristics of the inorganic crystal, it can freely pass through the crystal and be collected as a signal in the photomultiplier tube.

Scintillation detectors have a few advantages over semiconductor detectors such as HPGe. For instance, the light output response time of these detectors is much quicker than that of semiconductors, on the order of nanoseconds for scintillators vs hundreds of microseconds for semiconductors. This allows scintillators to operate at much higher count rates than semiconductors. Additionally, they operate at room temperature, and require no liquid nitrogen cooling. This increases utility as a field deployable or portable system. However, the primary disadvantage of scintillators is that their energy resolution is significantly worse than HPGe semiconductors.

$LaBr_3$:Ce is a relatively new scintillation material, and will be the primary detector type studied for much of this work, alongside HPGe detectors for comparison purposes. The below figure from (Gilmore, 2008) compares the properties of a number of different scintillation detector materials, including $LaBr_3$:Ce. The notable features are the relative conversion efficiency (vs NaI:Tl) and FWHM @ 661 keV. $LaBr_3$:Ce is the best detection material according to both of those metrics. Due to the promising characteristics of this material compared to most other modern scintillation materials, it was chosen for study in this work.

Scintillator	Activator	Abbreviation	Density ($g\,cm^{-3}$)	WL (nm)[b]	DCT (ns)[c]	RI[d]	RCE[e] (%)	After glow (%)[f]	Hyg[g]	FWHM[h] (%)
Sodium iodide	Tl	NaI(Tl)	3.67	415	230	1.85	100	0.3–5.0	Y	7.0
Caesium iodide	Tl	CsI(Tl)	4.51	550	1000	1.79	45	0.5–5.0	Y	—
	Na	CsI(Na)	4.51	420	630	1.84	85	0.5–5.0	S	7.5
	—	CsI	4.51	315	16	1.95	4–6	—	Y	—
Caesium fluoride	—	CsF	4.64	390	3–5	1.48	5–7	0.003–0.060	S	—
Calcium fluoride	Eu	CaF_2(Eu)	3.18	435	940	1.47	50	< 0.30	Y	—
Barium fluoride	—	BaF_2	4.88	310	630 + 0.6	1.50	16+5	—	N	—
Bismuth germanate	—	BGO	7.13	480	300 + 60	2.15	15–20	0.005	N	> 10
Cadmium tungstate	—	$CdWO_4$	7.90	540	5000	2.3	40	0.10	N	—
Lanthanum Chloride	Ce	$LaCl_3$(Ce)	3.79	350	28	~1.9	130	—	Y	3.8
Lanthanum Bromide	Ce	$LaBr_3$(Ce)	5.29	380	16	~1.9	160	—	Y	2.7
Gadolinium silicate	Ce	GSO	7.13	430	30–60	1.85	20	—	N	—
Lutecium silicate	Ce	LSO	7.4	420	40	1.82	40–75	—	N	—
Yttrium aluminium perovskite	Ce	YAP	5.37	347	28	1.94	40	—	N	—

[a] Data are taken from the Harshaw QS Scintillation Detector Catalogue (March 1992) and Saint-Gobain Ceramics and Plastics Inc. Internet sources.
[b] Wavelength at maximum emission.
[c] Decay time.
[d] Refractive index.
[e] Relative conversion efficiency (relative to NaI(Te)), i.e. net detector output using a bialkali photomultiplier tube (PMT).
[f] Fraction of light emitted more than 6 ms after the initial fluorescence.
[g] Hygroscopic?: Y, yes; N, no; S, slightly.
[h] Quoted resolutions are quoted at 661.6 keV and are typical rather than definitive.

Figure 7: Properties of an array of different scintillation materials (Gilmore, 2008).

Chapter 3: Background, History, and Literature Review

GAMMA-GAMMA COINCIDENCE SPECTROSCOPY

Historical applications of gamma-gamma coincidence measurements are plentiful. Gamma-gamma coincidence can provide significantly reduced detection limits for radionuclides which characteristically decay with cascading gamma emissions. Gamma-gamma coincidence can be used to probe the nuclear structure and fundamental decay schemes of radionuclides with complex decay patterns. Gamma-gamma coincidence can also be used to characterize unique detector configurations. The following is a summary of a few existing works which demonstrate these various applications of gamma-gamma coincidence spectroscopy.

A procedure for correcting for Compton scattering events to determine full gamma-ray energy is proposed (Hofstadter & Mcintyre, 1950). For Compton Scattering events occurring in detector 1, some of the scattered photons will deposit their remaining energy in detector 2, which is located off-axis from the initial photon beam and detector 1. Therefore, gating off of detector 2 provides coincidence events for these Compton interactions, and the cumulative energy simultaneously deposited in both detectors should be equal to the energy of the initial gamma-ray. This procedure could even be applied to none monoenergetic gamma-ray beams, as each gamma-ray energy present in the beam will provide a unique pulse height distribution between coincidence events in the two detectors.

Coincidence measurements of beta and gamma-rays from ^{60}Co were utilized to accurately characterize the efficiency of a 4 pi proportional counter detector geometry (Gunnink, Colby, & Cobble, 1959). The use of beta-coincidence is particularly convenient in this application because beta particles are nearly guaranteed to be detected by a 4 pi detection enclosure due to their limited range in materials. Therefore, the fraction of beta particles that are detected in coincidence with a gamma-ray (which in theory should be 100% if the detector was 100% efficient) provides an indication of the intrinsic efficiency of the detector for gamma-rays of that particular energy.

An array of three Geiger-Muller detectors was used to observe triple coincidence measurements resulting from double Compton Scattering events (Barton & Michaelis, 1960). This

introduces complications to measurements of deep underground cosmic radiation, which relied on gamma-ray coincidences in an array of detectors resulting from cosmic radiation. It is recommended to utilize a four-detector array for detection of cosmic radiation, as a triple Compton Scattering event is much less probable than a double Compton Scattering event, and will therefore have a much smaller uncertainty introduction to cosmic ray measurements.

Gamma-gamma coincidence measurements were made with two 3" x 3" NaI:Tl crystals of high-purity bismuth to detect trace amounts of ^{64}Cu on the level of 30 ng/g (Kim, Speecke, & Hoste, 1965). Separate measurements were also made to detect trace amounts of ^{110}Ag and ^{124}Sb within high-purity bismuth, yielding detection limits on the order of ng/g. The reduction in background achieved by employing coincidence measurements compared to single detector measurements resulted in a relative detection sensitivity reduction from 8 ng/g to 0.05 ng/g for the set of irradiation time, neutron flux, and sample size utilized in the experiment.

Gamma-gamma coincidence counting was applied to neutron-activation analysis of chlorine samples (Bramlitt, 1966). Employing gamma-gamma coincidence measurements allowed for deconvolution of the chlorine signal from interfering radionuclides in the sample that were also activated by NAA. Chlorine concentrations of 10 ppb were determined with this method. Previous measurement techniques relied on spectral deconvolution of overlapping peaks, or creation of composite decay curves by collecting multiple spectra over time. Gamma-gamma coincidence measurements represent a large improvement in simplifying chlorine quantification.

Gamma-gamma coincidence measurements of ^{75}Se were utilized to perform three-dimensional measurements of activity volume distributions in a sample. By utilizing an array of detectors, each pair of detectors that simultaneously detects a coincidence event can be used to place constraints on the physical location of the coincidence emitting source (Schmitz-feuerhake, 1970). (Indeed, this is the same method that is utilized in modern-day positron emission topography with annihilation photons from ^{22}Na).

A feasibility study of neutron activation analysis radioisotope measurements with gamma-gamma coincidence lithium drifted germanium detectors was conducted via computer studies

(Pagden & Sutherland, 1970). It is pointed out that a standard sample consisting of all stable elements, once irradiated, will emit on the order of 4000 unique gamma-rays in the energy range of 0-2 MeV, which exceeds the resolving capabilities of a single Ge(Li) detector. Utilizing a coincidence detection system consisting of two Ge(Li) detectors is shown to improve the resolving capabilities of the system by its square.

Highly excited states of ^{97}Tc were generated by bombarding a metallic foil containing enriched ^{94}Zr with ^{6}Li ions from tandem accelerators to produce the reaction ^{94}Zr(^{6}Li,3n)^{97}Tc with excess energies ranging from 18 to 30 MeV (Kajrys, Irshad, et al., 1982; Kajrys, Landsberger, Lecomte, Paradis, & Monaro, 1982). The purpose of producing these excited states is to measure and elucidate the set of possible nuclear level schemes and spin states which ^{97}Tc is capable of populating while de-exciting. The nuclear level states were determined via a variety of measurement techniques including: singles gamma-ray spectra, neutron-gamma coincidence, and gamma-gamma coincidence measurements of the de-excitation gamma-rays associated with each transition. The time-correlation information that is available through coincidence measurements allows unambiguous identification of successive nuclear levels that occur on a particular branch of the decay scheme, as well as the conditional intensities of the different decay branches based on previous transitions.

A review of large arrays of Compton suppressed HPGe detection systems was conducted (Beausang & Simpson, 1996). It is shown that such systems are capable of contributing to experiments aimed at investigating nuclear structure and decay schemes. The sensitivities provided by large array coincidence measurements reach 10^{-5} of the total reaction intensity. A disadvantage of any HPGe based detection system is a poor peak-to-background ratio caused by incomplete energy absorption in the HPGe detector. For instance, a typical HPGe measurement of ^{60}Co will result in only 20% of detected photons depositing their full energy. This is typically solved by utilizing a surrounding anticoincidence active shield of NaI:Tl or some other high-efficiency material. A quantity called the resolving power is introduced, which is a useful metric to quantify

the performance of a coincidence detection system, and the improvement in the spectrum quality obtained by utilizing coincidence spectroscopy. The resolving power is given by:

$$R = \left(\frac{SE_\gamma}{\Delta E_\gamma^{final}} \right) PT$$

where ΔE_γ^{final} is the FWHM resolution of the relevant gamma-rays, PT is the peak-to-total ratio, and SE_γ is the average energy separation of consecutive gamma-ray transitions in the cascade. The resolving power is therefore a function of the properties of the detector and the particular radionuclide or gamma-ray cascade under consideration.

Gamma-gamma coincidence measurements were made following the inelastic scattering of monoenergetic neutrons produced from an accelerator (McGrath, Garrett, Villani, & Yates, 1999). The detection system consists of a neutron collimator and three HPGe gamma-ray detectors. Typical inelastic neutron scattering measurements have difficulty identifying particular radionuclides in a complex sample containing natural materials. This is because inelastic neutron scattering can result in the population of a variety of low-spin states in a statistical manner. The complexity with which these spin states are filled precludes unambiguous radionuclide identification via single gamma-ray detection events. However, utilizing gamma-gamma coincidence spectroscopy allows for unambiguous isotopic identification due to the multidimensionality of the provided energy information. The measurement of coincident gamma-rays also allows for the construction of level schemes because the radionuclides emit cascading gamma-rays as they de-excite and pass through many energy levels. This coincidence measurement therefore provides both spectroscopic information regarding the contents of the natural sample, as well as additional information on the fundamental nuclear structure of the level schemes of the excited nuclear states as they de-excite.

Monte Carlo simulations of detector response are compared to experimental data from prompt gamma-gamma coincidence measurements with NaI:Tl scintillators in order to validate the

variance reduction techniques and detector response functions employed in the simulation (Metwally, Gardner, & Sood, 2007). The use of detector response functions speeds up computation time by replacing the statistical tracking of individual gamma-rays within the detector with individual gamma-ray spectra that correspond to what the detector would output in response to a gamma-ray of an initial energy. These individual gamma-ray spectra are superimposed on each other for each initial gamma-ray energy that is incident on the detector in order to generate the resulting composite gamma-ray spectrum. However, for radionuclides which decay with cascading gamma-ray emissions, determining the individual energies of each incident gamma-ray can be difficult when validating a detector response function. Fortunately, gamma-gamma coincidence measurements allow for deconvolution of these cascading emissions, and are capable of isolating each incident gamma-ray energy. The experimental data from measurements of natural mercury and nickel were compared to simulated detector response functions. The coincidence gates were shown to agree well between experimental and simulated data for the expected coincidences. However, the experimental data had additional low-energy chance coincidences.

Coincidence events consisting of two or more gamma-rays are utilized to perform measurements of nuclear waste analysis, neutron activation analysis, and prompt gamma-ray analysis. Nuclear waste was simulated using a sample containing approximately 1 microCurie each of ^{94}Nb, ^{108m}Ag, ^{152}Eu, ^{166m}Ho, and approximately 20 microCuries of ^{60}Co. After 50,000 seconds of coincident data acquisition, detection limits for each of the 1 microCurie samples are determined to be on the order of 2-3 Bq. An example of gamma coincidence NAA measurements is determination of environmental iridium concentrations (Oshima et al., 2008). Gamma coincidence NAA is capable of detecting the approximately 10 fg/g concentration of iridium, which is indicative of meteorites influencing the environment of the earth. Gamma coincidence prompt gamma analysis can also be applied for cadmium analysis of plastic and food samples. This method should be capable of sub-ppm detection limits in plastic and food samples.

Gamma-gamma coincidence was employed for measurements of selenium in biological samples subject to NAA (Piero, Bacchi, & Fernandes, 2008). The detection system was an HPGe

detector and NaI:Tl shield, which was capable of producing both coincidence and anticoincidence spectra. The developed method reduced the detection limit of selenium by a factor of 2-3. Uncertainty was also further constrained compared to previous methodology.

A gamma-gamma coincidence spectrometer was constructed with two HPGe detectors with applications in coincidence NAA and characterization of reference materials (Tomlin, Zeisler, & Lindstrom, 2008). This paper points out an important limitation of coincidence performance. A typical metric used to compare singles and coincidence spectra is the peak-to-background ratio, sometimes referred to as the signal-to-noise ratio. In nearly all measurements of cascading gamma-rays, coincidence counting results in an improvement to the signal-to-noise ratio. However, due to the significantly lower efficiency of coincidence counting, the peak area of the photopeak is significantly reduced. In some cases, the loss of peak counts can lead to an increase in the uncertainty in peak area that outweighs the uncertainty reduction achieved by suppressing background count. It is therefore important to consider not only the signal-to-noise ratio, but also the peak area and its relative uncertainty when comparing performance between single detectors and coincidence detection systems.

A gamma-gamma coincidence spectrometer was developed at a tangential neutron beam port at the Dalat Nuclear Research Reactor. Characterization of the system was performed using ^{60}Co and $^{35}Cl(n,2n)^{36}Cl$ reactions (Khang, Hai, Tan, & Dien, 2011). This system is intended for applications including neutron activation analysis and nuclear structure studies.

Neutron activation analysis was used to measure trace amounts of mercury and selenium in biological samples (Horne & Landsberger, 2011). Complications arise due to the interfering gamma-ray emissions between ^{203}Hg and ^{75}Se, which is an activated product of natural selenium. To de-convolute these overlapping peaks Compton suppression was employed. The interfering peak from ^{75}Se is part of a cascading emission, and is thus eliminated from the spectrum of an anticoincidence/Compton suppressed data acquisition. Furthermore, coincidence gating was employed to eliminate background and bremsstrahlung interference, which results from activated

^{32}P. As a result of these gating techniques, mercury and selenium concentrations were successfully determined in a set of standard reference materials.

A NaI:Tl gamma-gamma coincidence detection system was developed for isotopic analysis of uranium with gamma-ray and x-ray fluorescence coincidence (Zhang et al., 2011). Gamma-gamma coincidence measurements were taken for uranium standards with enrichments varying from depleted uranium to weapons grade uranium. Qualitative differences between the coincidence heatmaps of varying enrichment level samples were discussed, but no quantitative assay was possible due to the strong interferences from detector cross-talk and x-ray fluorescence resulting in random coincidences.

Measurements of aerosol samples were made using both single and coincidence HPGe detector systems (Konki et al., 2012). The background activity level has been varied between coincidence data acquisitions, while low background has been preserved in the single detector configuration. The performance of single vs coincidence measurements is compared as a function of coincidence background radiation level. Minimum detectable activities of all investigated radionuclides (^{22}Na, ^{60}Co, ^{99}Mo, ^{134}Cs, and ^{140}La) are improved by employing coincidence counting. It is found that gamma coincidence counting is useful for aerosol filter analysis, especially in cases of elevated background.

A procedure was developed for characterization of the total detector efficiency using gamma-gamma coincidence measurements (Erikson et al., 2013). A typical peak efficiency calibration considers only the gamma-rays that result in a full-energy deposition in the detector. By contrast, the total detect efficiency considers both the gamma-rays that deposit their full energy in one event, as well as Compton Scattering events which result in partial energy deposition. Gamma-gamma coincidence allows the Compton continuum to be isolated from the rest of the spectrum, as it is mapped as a diagonal streak across the two-dimensional gamma-gamma coincidence plane. Therefore, collecting measurements in coincidence allows for total detector efficiency characterization via measurement of the two-dimensional Compton continuum in coincidence spectroscopy.

Gamma-gamma coincidence/anticoincidence was utilized for determination of low-level cosmogenic ^{22}Na and ^{7}Be in air-filter samples (Zhang, Ungar, Stukel, & Mekarski, 2014). Measurements of these two radionuclides are potentially useful as a tracer and radiochronometer of lower stratosphere or upper troposphere air masses. They can also be used to measure ice sheet hydrology through river samples. However, current techniques for measuring trace quantities of ^{22}Na are unreliable. This paper developed an improved method for measuring ^{22}Na via measurements of the 511 keV annihilation photons in coincidence with BGO scintillators. Measurement of the ^{7}Be 477.6 keV photon was performed via anticoincidence to eliminate the effects of the Compton continuum. The critical limits for these two radionuclides after a 20-hour count reached 3 mBq and 5 Bq for ^{22}Na and ^{7}Be respectively. This represents a significant improvement on existing techniques which relied on a single HPGe spectrometer.

Gamma-gamma coincidence is used to determine selenium in coal fly ash subject to NAA (Yoho & Landsberger, 2015). Gamma-gamma coincidence successfully reduces the high Compton backgrounds in this spectrum, as well as interferences from gamma-ray peaks from ^{180}Hf and ^{182}Ta. Corrections are made for dead-time and random-summing. The calculated selenium concentrations in fly-ash and certified reference materials agree with the certified values.

A method was developed for quantifying coincidence signatures with a custom-built software package that includes corrections for efficiency and cascade summing (Britton, Jackson, & Davies, 2015). The detectors utilized were planar HPGe detectors. This system was compared to results from a single detector, and found to provide accurate results for measurements of ^{60}Co, ^{88}Y, ^{103}Ru, ^{133}Ba, ^{140}Ba, and ^{140}La.

A dual coincidence/anticoincidence digital HPGe detector system was characterized for measurements of environmental samples (Markovic, Roos, & Nielsen, 2016). Comparisons of minimum detectable activity (MDA) were made for measurements of ^{210}Pb in a uranium certified reference material and ^{134}Cs in a matrix of large ^{137}Cs activity between single and coincident detector systems. In all cases, coincidence measurements had a lower MDA than single detector results. This primarily results from the significant background reduction resulting from

coincidence gating. In particular, narrow energy window gates of coincidence measurements provide an even stronger MDA improvement than full window coincidence gates.

CERIUM-DOPED LANTHANUM BROMIDE DETECTORS

A survey of the properties and applications of lanthanum bromide scintillation detectors was conducted (Iltis et al., 2006). Comparisons were made to existing scintillator technology such as NaI:Tl. $LaBr_3$:Ce was shown to be the brightest scintillator at 63,000 photons/MeV. $LaBr_3$:Ce is stable (emits 90% of that light) at temperatures up to 175 C. The detectors have sub nanosecond coincidence resolving times. The detectors can handle count rates of at least 1.8 Mcps due to the 30 nanosecond pulse decay time. Sizes up to 3" x 3" are available.

Gamma-gamma coincidence measurements were made with a mixed array of HPGe and $LaBr_3$:Ce detectors to study the nuclear structure of $^{33, 34}P$ and ^{33}P following fusion-evaporation reactions between an ^{18}O beam and an isotopically enriched ^{18}O implanted tantalum target (Alharbi et al., 2012). The excellent timing performance of $LaBr_3$:Ce detectors allowed for measurements of phenomena in the pico-to-nanosecond time regime. The lifetime of the first negative parity state in the N = 19 isotone ^{34}P was measured using the $LaBr_3$:Ce gamma-gamma coincidence system. A half-life of 2 ns for an electromagnetic transition rate in ^{34}P was established. The lifetime measurements were shown to be consistent with single-particle M2 multipolarity associate with a $f_{7/2}$->$d_{5/2}$ single particle transition.

A Compton suppressed $LaBr_3$:Ce detection system was used to perform nondestructive assay on spent nuclear fuel (Bender, Heidrich, & Ünlü, 2015). The resulting gamma-ray spectrum was compared to the results from HPGe and NaI:Tl detection systems both with and without Compton suppression, as well as a single unsuppressed $LaBr_3$:Ce detector. The performance of each system was investigated in terms of the total number of resolvable and identifiable peaks, as well as the peak-to-Compton ratios of each system with and without Compton suppression. It was shown that performing Compton suppression results in suppression factors (the ratio of peak-to-Compton ratios of suppressed vs unsuppressed measurements with each detector) on the order of

approximately 2 for the HPGe and $LaBr_3$:Ce detection systems. These measurements demonstrate that $LaBr_3$:Ce detection systems benefit significantly from Compton suppression when performing measurements of spent nuclear fuel, which are frequently obscured by the Compton continuums from ^{137}Cs and ^{140}La. The primary advantage of employing $LaBr_3$:Ce systems as opposed to HPGe systems is the low maintenance and ability to operate at room temperature. The primary difficulty in Compton suppression of a high activity sample such as spent nuclear fuel is that the enclosed geometry creates significant losses in the net areas of large photopeaks, introduction of additional sum peaks, and losses to randomly suppressed counts.

FISSION PRODUCT MEASUREMENTS

Measurement of fission products is a commonly employed technique for the nondestructive assay and verification of spent nuclear fuel. It is important to quantify the presence of fission products in spent nuclear fuel in order to verify that the condition of the fuel is consistent with its declared lifetime operating history. The measured fission product contents can be used to determine the initial enrichment, burnup, and a variety of other properties of spent nuclear fuel.

Measurements of spent nuclear fuel were performed with gamma-ray spectroscopy to verify operator-declared data (Willman, Håkansson, Osifo, Bäcklin, & Svärd, 2006). The fission products that were measured include ^{137}Cs, ^{134}Cs, and ^{154}Eu. The half-lives of these three radionuclides are 30.1 years, 2.1 years, and 8.6 years respectively. These three radionuclides therefore dominate the gamma-ray spectrum of discharged fuel on the timescales corresponding to 10-20 years of cooling. These measurements were used to determine burnup and cooling time of SNF. Computer simulations in ORIGEN-ARP (Oak Ridge Isotope Generation Automatic Rapid Processing) provided estimates on the detection limits of deviations from operator-declare burnup and cooling time data. The measurements were also used to provide independent burnup and cooling time data when no operator-declared data was available. It may also be possible to verify the initial enrichment of the fuel via measurement of these three fission products.

Gamma-ray spectroscopy was used to determine the burnup of Material Testing Reactor fuel elements from the RP-10 research reactor (Mora, Padilla, Palomino, & Terremoto, 2011). The only fission product that was measured to determine burnup was ^{137}Cs. Corrections were made for self-attenuation of the 661 keV photons in the fuel element, attenuation in the water (measurements were made on site in the spent fuel reactor storage pool), and attenuation in aluminum cladding. A detector efficiency characterization was also performed exclusively for the 661 keV photon as a function of distance, such that the results can be integrated along the sample geometry during the experimental measurements. This measurement procedure yielded average burnup results that agreed with previous measurements and ORIGEN-ARP models. This measurement was successful even for spent fuel elements with cooling times as short as 106 days. This demonstrates that it is not necessary to wait two years to begin burnup measurements with ^{137}Cs.

Nondestructive assay measurements of spent nuclear fuel were performed to: verify initial fuel enrichment, burnup, and cooling time, detect the diversion or replacement of pins, estimate plutonium content, estimate decay heat, and determine the spent fuel reactivity (Vaccaro et al., 2016). These measurements will be performed with HPGe detector gamma-ray spectroscopy on photon emissions from ^{137}Cs, ^{154}Eu, and ^{134}Cs for 50 different fuel assemblies. Results were also compared to a limited number of ORIGEN-ARP simulations. The ^{154}Eu/^{137}Cs ratio is known to vary nearly linearly with fuel burnup under 35 GWd/tU, and was therefore measured to infer the fuel burnup of each assembly. This study also generated a large library of gamma spectroscopic datasets representing known fuel compositions, which can aid further measurements of irradiated fuel verification.

Gamma-ray spectroscopy with a CdZnTe detector was used for characterization of spent nuclear fuel. Determination of the enrichment of uranium was achieved to within 10% of the declared values (Abbas, Morel, Etcheverry, & Nicolaou, 1998).

Chapter 4: Experimental Setup

APPARATUS

The Nuclear Engineering Teaching Lab (NETL) at The University of Texas at Austin (UT Austin) has obtained two identical Saint Gobain Brillance 380 $LaBr_3$:Ce scintillation detectors with 38 mm x 38 mm cylindrical crystals and AS20 voltage dividers with analog signal output for use in a coincidence configuration. It should be noted that Saint Gobain currently offers Brillance 380 LaBr3:Ce scintillation detectors at sizes up to 76 mm x 76 mm, which would have significantly higher efficiency than the $LaBr_3$:Ce detectors utilized here. NETL is also equipped with two HPGe detectors in a coincidence configuration. Coincidence data processing was achieved with an XIA LLC Digital Gamma Finder Pixie-4 card. The DGF Pixie-4 is a multichannel data acquisition system for coincident radiation detection which assigns timestamps with a 13.3 ns timing resolution to each detected event (XIA LLC, 2013). This unit is capable of controlling many aspects of signal processing and shaping through digital controls in the Igor Pro interface, which almost completely eliminates the need for a NIM bin of modules with analog controls. Significant effort has been expended to optimize all adjustable parameters of the software to maximize the performance of the detectors.

The following figure is a block diagram of the experimental setup for the coincidence $LaBr_3$:Ce detectors. The block diagram for HPGe detectors has no practical difference and is excluded.

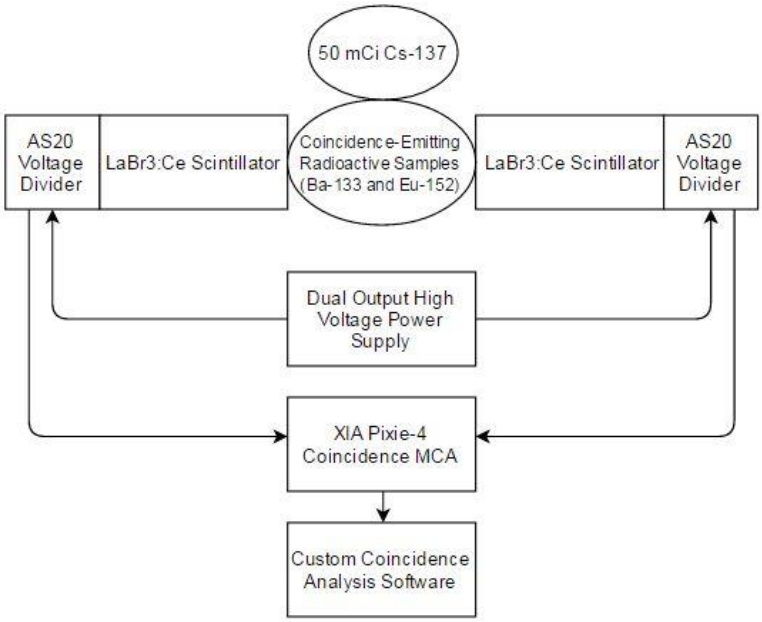

Figure 8: $LaBr_3$:Ce coincidence block diagram.

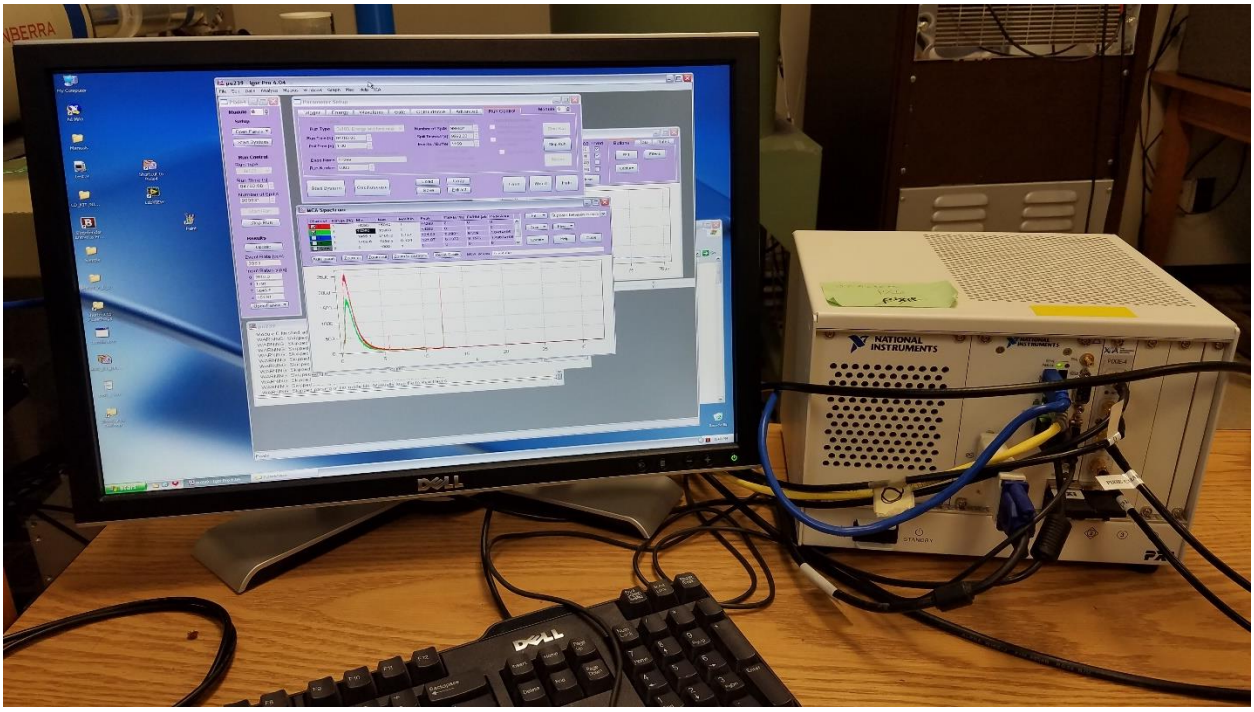

Figure 9: The Pixie computer with the XIA LLC Pixie-4 coincidence module installed. Displayed on the screen is the Igor Pro program.

The data collection interface is the Igor Pro program that operates the XIA Pixie-4 system. The software includes an adjustable coincidence timing window, which specifies the maximum time between two events that are registered as coincident. A procedure for optimizing the coincidence timing window for each detector type was developed, and will be presented. The manufacturer of the $LaBr_3$:Ce detectors list the efficiency as 143% vs NaI:Tl and optimum energy resolution as 2.1% at 1332.5 keV, as opposed to the 5.4% energy resolution of NaI:Tl at the same energy (Saint Gobain, 2009).

SYSTEM CHARACTERIZATION OVERVIEW

Complete characterization of the performance of the $LaBr_3$:Ce coincident detector arrangement will be divided into a series of separate experiments, many of which will include comparisons to established detection and/or modelling technology. The set of experiments which were performed to characterize the system are outlined below:

1. Timing performance characterization of the detectors. This included determination of the optimum timing window for gamma-gamma coincidence measurements, and of the detector response time to radiation events via analysis of the oscilloscope readouts from the $LaBr_3$:Ce detectors, and comparisons to oscilloscope readouts from HPGe detectors.
2. Efficiency and energy resolution measurements were performed for both the $LaBr_3$:Ce detectors and the HPGe detectors. The results will also be compared to MCNP simulations.
3. MCNP6 simulations on measurement of a collection of point sources utilizing a single $LaBr_3$:Ce detector, and the results will be compared to experimental results, in order to benchmark the performance of the system, determine the capabilities of the system to improve through further optimization, and discuss any shortcomings of simulations that may exist.
4. Background elimination via coincidence gating was performed on the $LaBr_3$:Ce detectors to demonstrate the capabilities of gamma-gamma coincidence to eliminate noncoincident

events from a resulting gamma-ray spectrum, and alleviate the shortcomings of $LaBr_3$:Ce detectors due to their intrinsic radioactivity.

5. Single and dual detector peak signal-to-noise (SNR) ratio determinations were made for a test case of measurements of several radionuclides for both $LaBr_3$:Ce and HPGe detectors. This provided comparators to quantify the performance of coincident $LaBr_3$:Ce detectors in a plausible, realistic, and challenging measurement scenario.
6. Measurements of a collection of irradiated uranium reference materials of varying enrichment levels were made. This simulated a potential high count-rate nuclear safeguards application of coincident $LaBr_3$:Ce detectors such as measurement of highly active spent nuclear fuel rods. Identification of a few of the fission products present in the spectrum will be performed, and qualitative differences between the coincidence heatmaps resulting from uranium of differing enrichments are discussed. The time evolution of the coincidence heatmaps post-irradiation was investigated via a series of measurements made over the course of a month following initial sample irradiations.

Chapter 5: Results and Data Analysis

Data were collected in order to compare the following properties of $LaBr_3$:Ce and HPGe detectors: timing performance, efficiency, energy resolution, similarity to simulation results, background elimination via coincidence gating, single detector and coincidence configuration peak signal-to-noise ratio (SNR). $LaBr_3$:Ce detectors were also utilized for the analysis of coincident fission product spectra from irradiated uranium samples of varying enrichments as an analog measurement for real-world in-situ measurements of spent nuclear fuel.

TIMING PERFORMANCE

Timing performance of the two detector types was compared by counting a ^{60}Co source while varying the adjustable coincidence timing window setting in the Igor Pro software. According to the decay structure of ^{60}Co, the 1173.2 keV gamma-ray in coincidence with 1332.5 keV gamma-ray represents a true coincident event, while 1173.2 keV gamma-ray in coincidence with itself, or 1332.5 keV gamma-ray in coincidence with itself represents a false coincidence event, as seen in the figure of its decay scheme below.

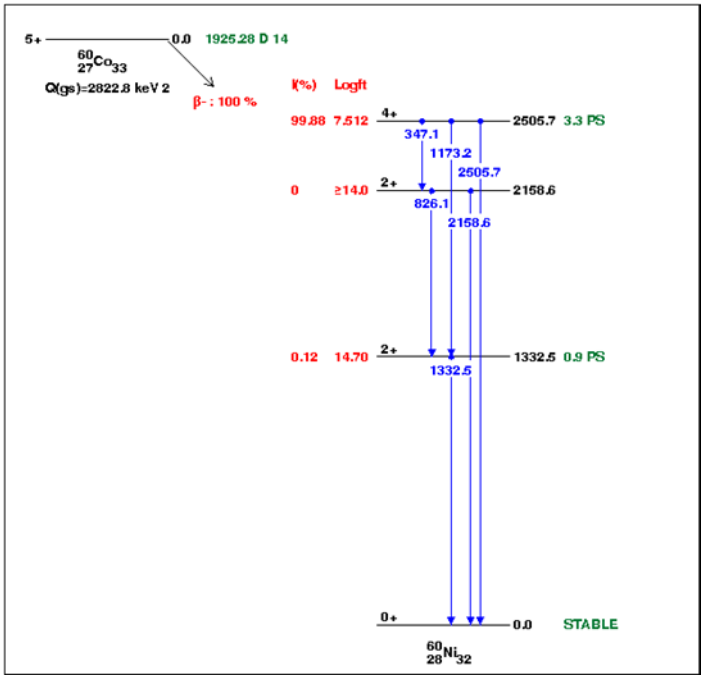

Figure 10: The decay scheme of ^{60}Co.

Therefore, comparing the magnitude of peaks at true and false coincidence energy coordinates as seen in Figure 11 provides an SNR, which is a useful metric to quantify the coincidence timing performance of each detector type for a range of timing window settings, and thus determine the optimum timing window setting for each detector type. The left panel of Figure 11 shows the coincidence heatmap with a 13 ns timing window. The right panel of Figure 11 shows the coincidence heatmap with a 500 ns timing window. Note the increased clustering of random coincidences at (1332, 1332) present in the 500 ns timing window heatmap.

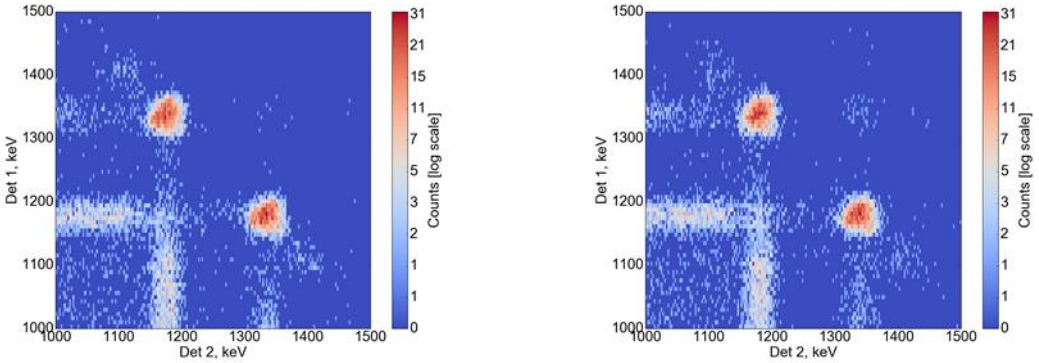

Figure 11: ^{60}Co coincidence heatmap. Left: 13 ns timing window. Right: 500 ns timing window. The energy coordinates at (1173, 1173) and (1332, 1332) represent false (random) coincidence events, while (1173, 1332) and (1332, 1173) represent true coincidence events.

The above figure shows the results from measuring this SNR at varying timing windows. The optimum coincidence windows for HPGe and $LaBr_3$:Ce detectors are 26.6 and 13.3 ns respectively. It should be noted that the XIA Pixie-4 is only capable of producing timing windows with a resolution of 13.3 ns. It is therefore likely that the optimum $LaBr_3$:Ce timing windows was not achieved, and exceeds the capabilities of current instrumentation. There exists an XIA Digital Gamma Finder Pixie-500 with a clock of 500 MHz. If acquired, it is expected that this would significantly improve the performance of the $LaBr_3$:Ce detectors. The performance of HPGe detectors on the other hand was optimized at about 26 ns, and dropped considerably when reducing the timing window from 26.6 ns to 13.3 ns. These timing windows were used for all coincident SNR comparisons between the two detector types that follow.

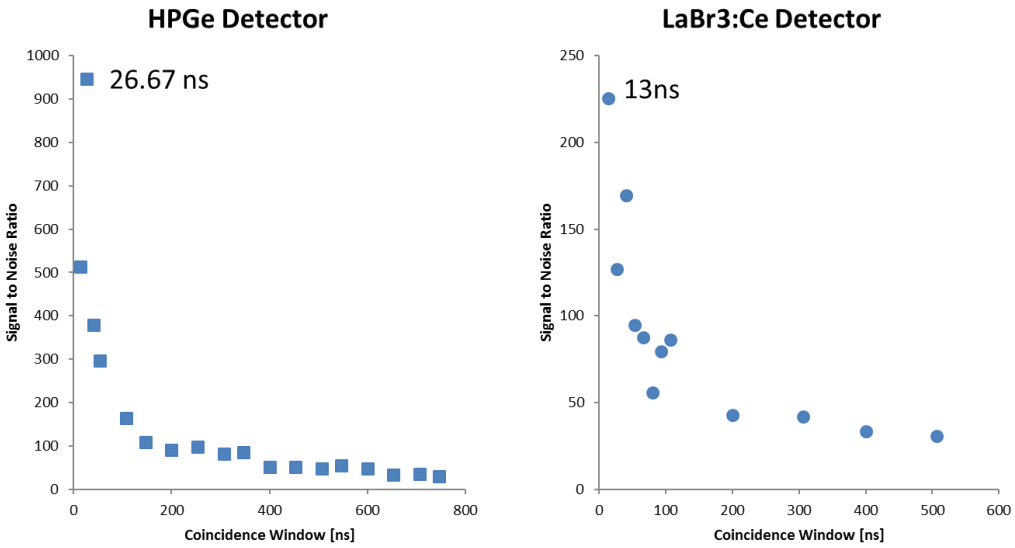

Figure 12: SNR vs coincidence timing window for the HPGe and $LaBr_3$:Ce detectors.

Another important metric related to the timing performance of a radiation detector is its signal response over time to a radiation event. Comparisons were made between the oscilloscope readouts of the HPGe and $LaBr_3$:Ce detectors in order to predict their capabilities in high count-rate regimes. The oscilloscope readouts from these two types of detectors are shown in Figures 13-15 below. It is seen that the HPGe detector signal takes approximately 140 μs to return to its base level. By comparison, the signal from the $LaBr_3$:Ce detector returns to its baseline level on the order of about 2 μs. The significantly faster response time of $LaBr_3$:Ce detectors will allow for handling of much higher count rates with lower dead-times than HPGe detectors. This was further investigated. It should be noted that the Pixie-4 module utilized for data acquisition is capable of recording events with dead times as low as 1 μs per event. The HPGe detectors therefore represent a significant bottleneck in an effort to develop a high count-rate data acquisition system.

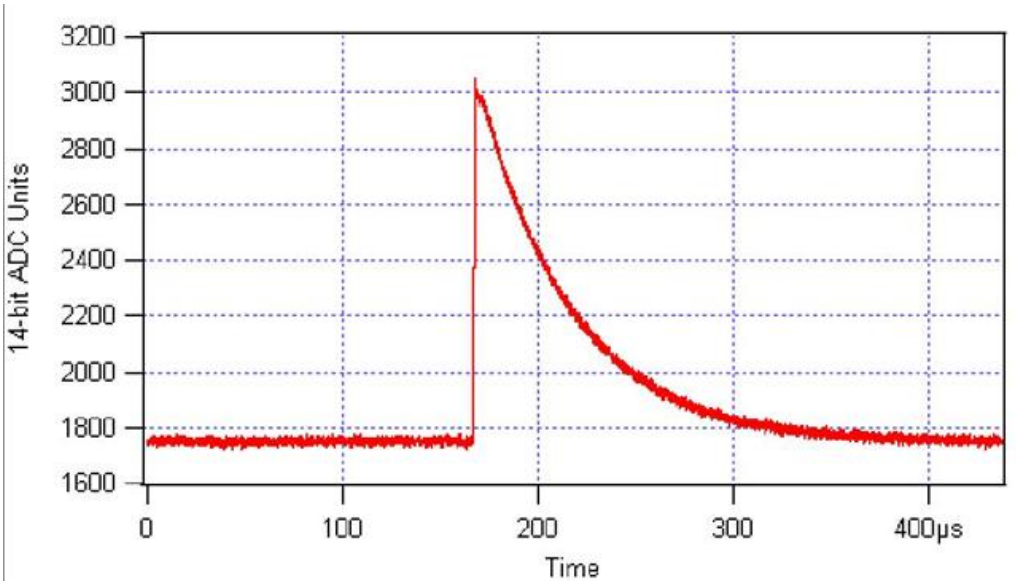

Figure 13: Oscilloscope readout of HPGe detector response.

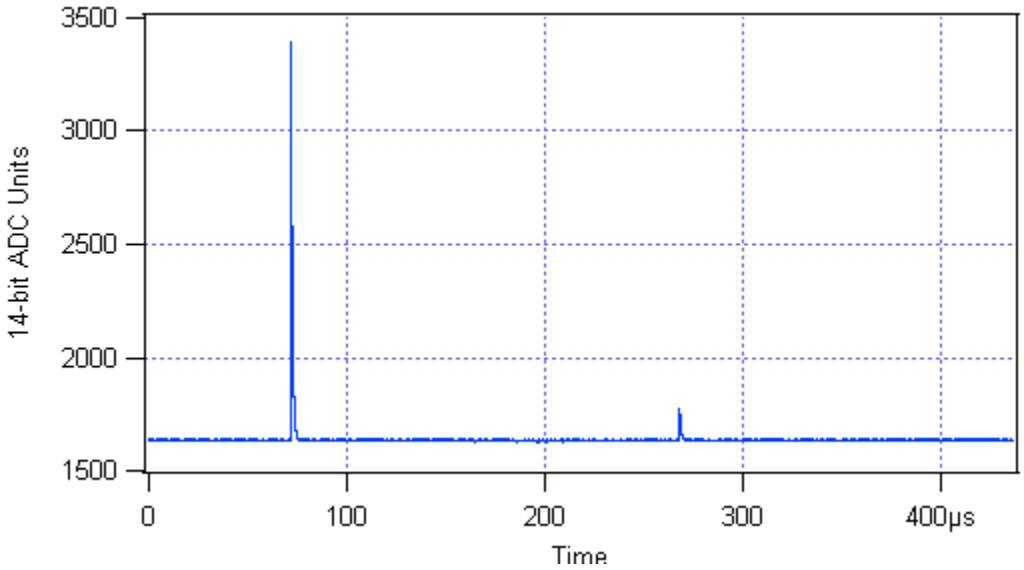

Figure 14: Oscilloscope readout of LaBr:Ce detector response

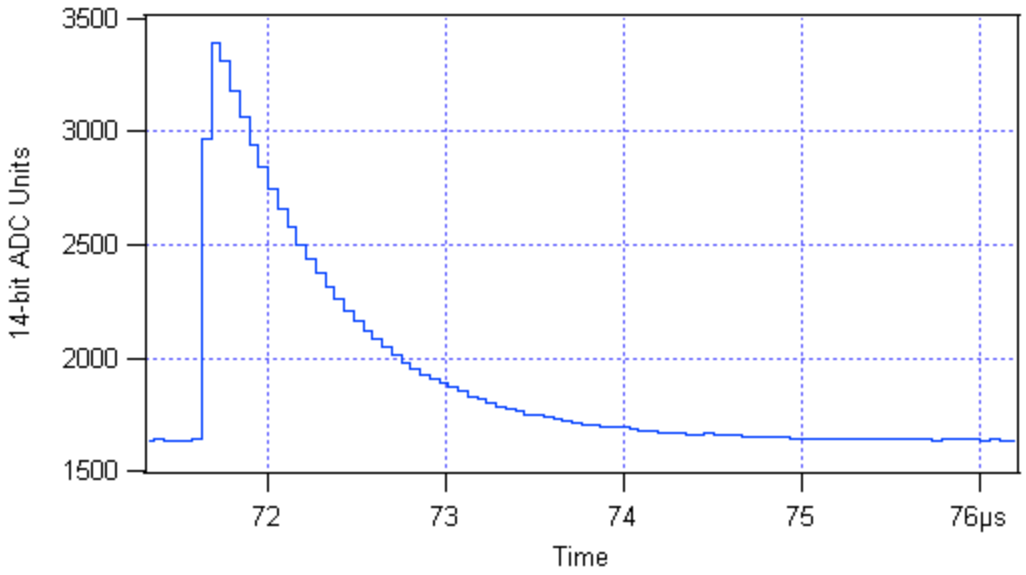

Figure 15: Zoomed-in oscilloscope readout of $LaBr_3$:Ce detector response.

EFFICIENCY AND ENERGY RESOLUTION

A collection of certified monoenergetic gamma sources was utilized in the determination of detector efficiency and energy resolution. These sources were provided by Eckert & Ziegler, and include ^{241}Am, ^{109}Cd, ^{139}Ce, ^{203}Hg, ^{113}Sn, ^{137}Cs, ^{54}Mn, ^{65}Zn, and ^{60}Co. Each source was counted on each detector at a distance of 10 cm for 300 seconds. This distance was chosen in order to minimize dead-time and pile-up while still maintaining Gaussian peaks with a net area of at least 3,000 counts. The geometry of the counting setup was preserved between the two detector types. The activities of all sources were below 1 µCi, therefore dead-time and true coincidence summing effects were negligible. The HPGe detector utilized was a GMX35P4-70 n-type cylindrical detector with dimensions of 55.9 mm x 57.5 mm.

Absolute full-energy detector efficiency was determined by calculating the net area of each photopeak using ORTEC Maestro's built-in peak identification functionality, and comparing the result to the total number of expected emissions of photons of that energy from the monoenergetic sample during the data acquisition time. This calculation requires consideration of the activity of the sample, the age of the sample, the half-life, and the intensity of that particular photon energy. Absolute full-energy detector efficiency is thus calculated according to the equation:

$$\varepsilon = \frac{C_{net}}{A_0 \times \frac{1}{2}^{T/T_{1/2}} \times I \times t}$$

In this equation, ε is the absolute full-energy detector efficiency, C_{net} is the net area of the main photopeak from the gamma source, A_0 is the activity of the gamma source when it was created, T is the time since source creation, $T_{1/2}$ is the half-life of the gamma source radionuclide, t is the data acquisition time, and I is the intensity of that particular photopeak emission. The results of these calculations for each primary photopeak from each source, for both detectors, is given in Figure 16 below. Uncertainty has also been propagated and is presented with error bars representing one sigma.

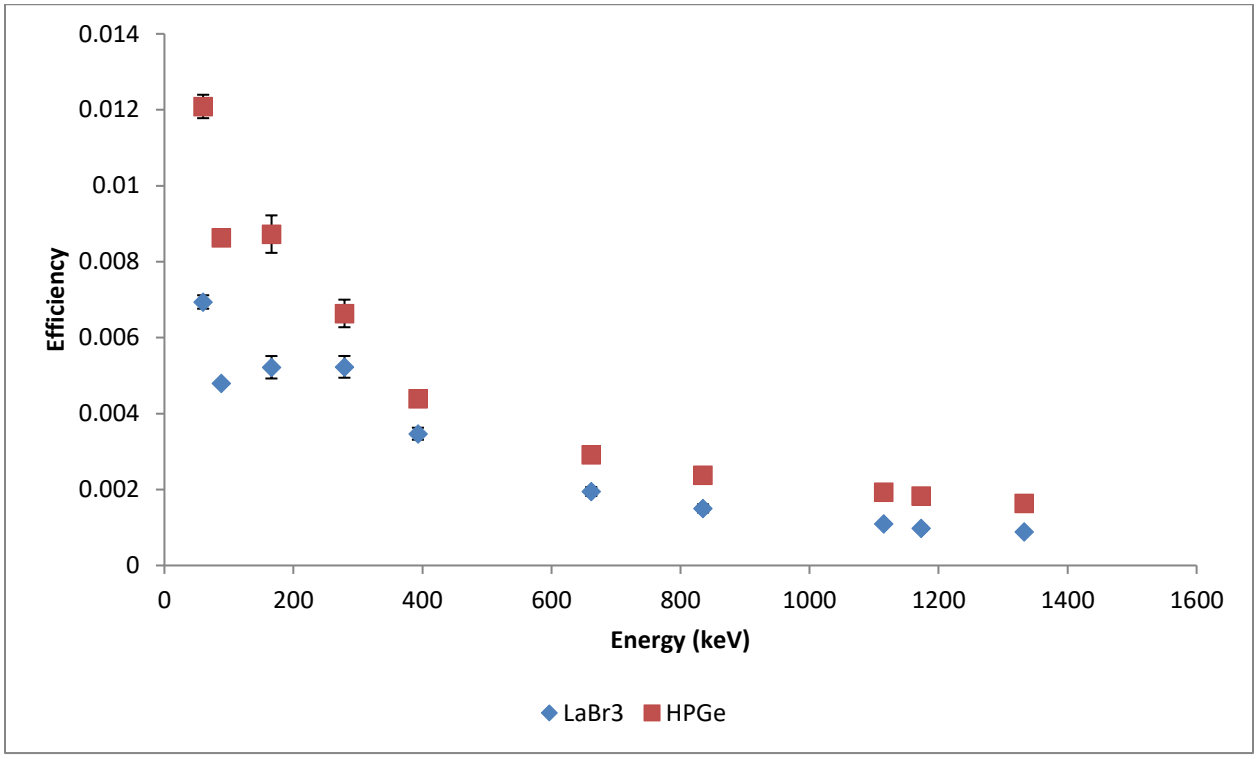

Figure 16: A comparison of the efficiency of $LaBr_3$:Ce and HPGe detectors.

The efficiency results for the $LaBr_3$:Ce detector were also compared to MCNP6 simulations. The MCNP6 simulation utilized a gamma-ray source term that included all of the energies that were experimentally measured, in order to obtain efficiency results at the same points

for easier comparison. The simulation ran 10 million particles to achieve uncertainties on the order of 1%. The results were post-processed to subtract background and obtain net areas for each photopeak, and uncertainty was propagated throughout. The results are shown in comparison to experimental results in the following figure. Uncertainty bars are provided on all MCNP data points, but most of them are smaller than the data points themselves. The notable exception is in the low-energy regime, where there are both substantial uncertainties and disagreement with experimental results. This is likely due to the large number of interactions that are possible for low energy gamma-rays, some of which may not have been accurately tracked by MCNP. The MCNP code for this efficiency determination is included in the appendix of this work. The efficiency data and associated error bars presented here for the experimental $LaBr_3$:Ce detectors are identical to the data presented previously in the comparison of $LaBr_3$:Ce and HPGe efficiency. This comparison is shown in Figure 17.

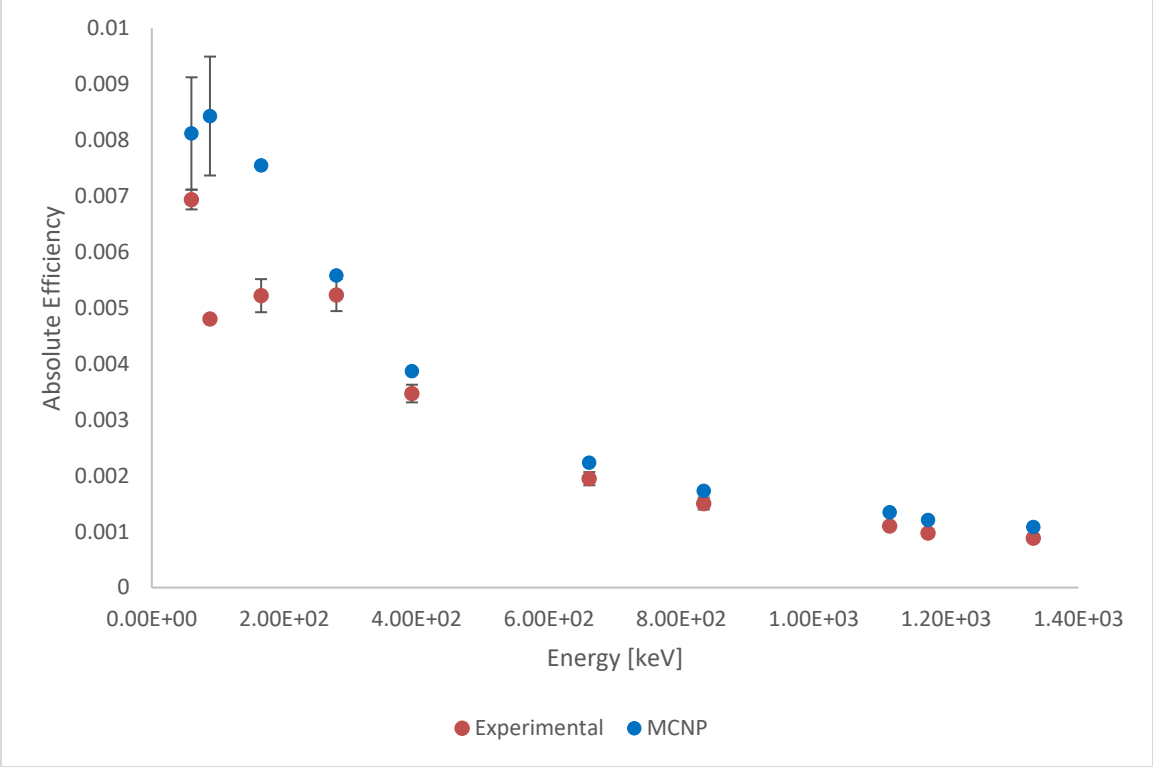

Figure 17: $LaBr_3$:Ce efficiency characterization results from experiment and MCNP.

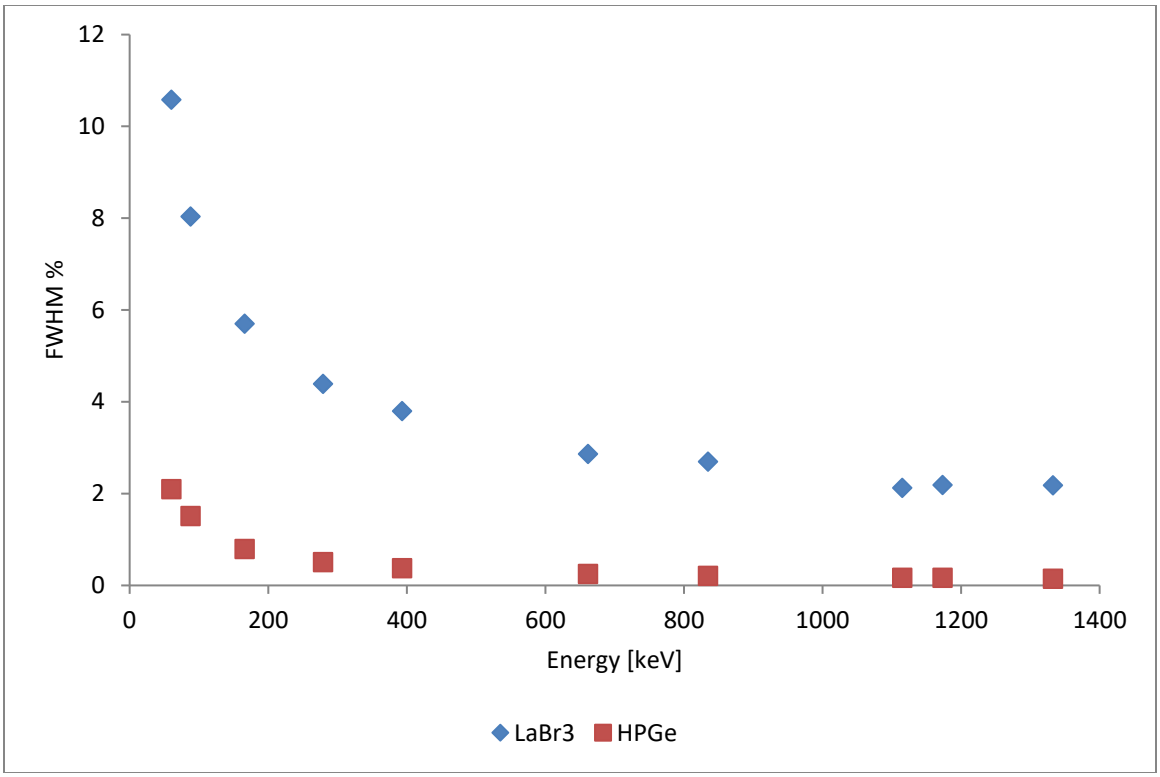

Figure 18: A comparison of the energy resolution of $LaBr_3$:Ce and HPGe detectors.

Figure 18 shows the comparison of energy resolution between LaBr3:Ce and HPGe detectors. The HPGe detector has superior energy resolution to the $LaBr_3$:Ce detector. Energy resolution values were obtained using ORTEC Maestro's built-in peak identification functionality in order to identify the peak locations and full-width half maximum (FWHM) values. Energy resolution is defined as the ratio of the FWHM of the photopeak to the energy of the peak centroid, expressed as a percentage:

$$ER = \frac{FWHM}{E_{peak}} \times 100$$

where ER is the energy resolution, FWHM is the full-width half max of the photopeak in [keV], and E_{peak} is the energy of the peak centroid.

MCNP6 SIMULATIONS

Additionally, performance of a single $LaBr_3$:Ce detection system was validated via comparison to Monte Carlo simulations in MCNP6. A comparison of experimental detector response to simulations was conducted for the simple scenario of $LaBr_3$:Ce detectors measuring a set of gamma-emitting sources including ^{60}Co, ^{22}Na, and ^{137}Cs. The code is given in the appendix of this work for reference.

In order to create a realistic detector response spectrum with MCNP6 simulations, it is necessary to include a description of the energy resolution of the detector using the Gaussian Energy Broadening (GEB) function. Gaussian Energy Broadening is a tool in MCNP6 that increases the full-width half maximum of peaks in the gamma-ray spectrum to match the response of a detector. It takes three numerical inputs a, b, and c, to match the energy resolution in terms of FWHM [MeV] of the detector to an energy-dependent [MeV] function of the form:

$$FWHM = a + b\sqrt{E + cE^2}$$

The energy resolution of the $LaBr_3$:Ce detectors as shown in Figure 19 was matched to this function with the following parameters:

$$FWHM = 0.001 + 0.0205 * \sqrt{E + 0.3 * E^2}$$

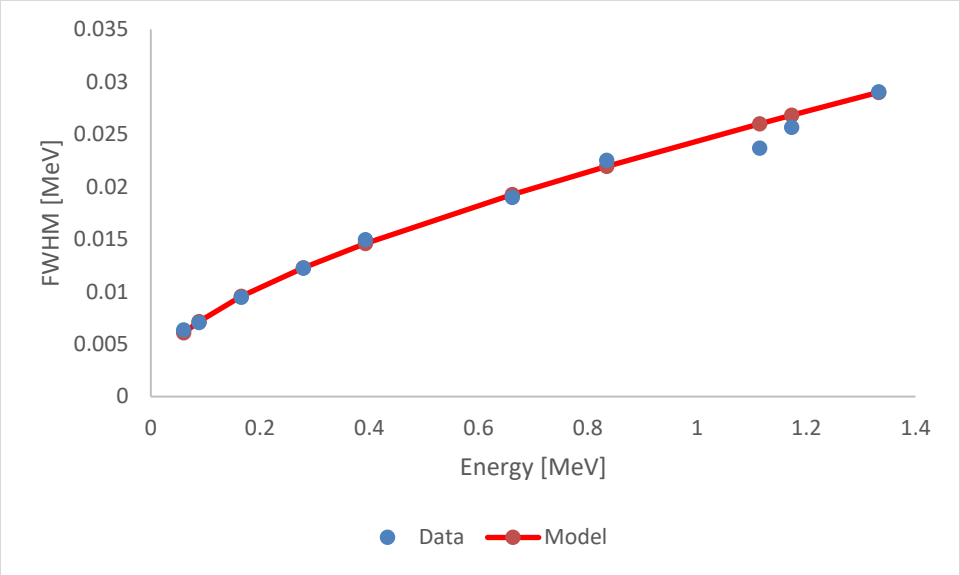

Figure 19: The energy resolution model which provided the parameters for the GEB card in MCNP6.

To simulate the experimental measurement of the three test sources ^{22}Na, ^{137}Cs, and ^{60}Co, three separate MCNP6 runs were conducted. Each MCNP6 run took approximately two hours and was performed with 10^5 particles. By separating the measurements of each source in MCNP6, the data was able to be post-processed to weight the spectral contributions from each source according to the relative activities present in the experimental measurement. This allowed for the creation of a composite gamma-ray spectrum that closely matches the experimentally observed spectrum. A comparison of the two spectra is given in Figure 20.

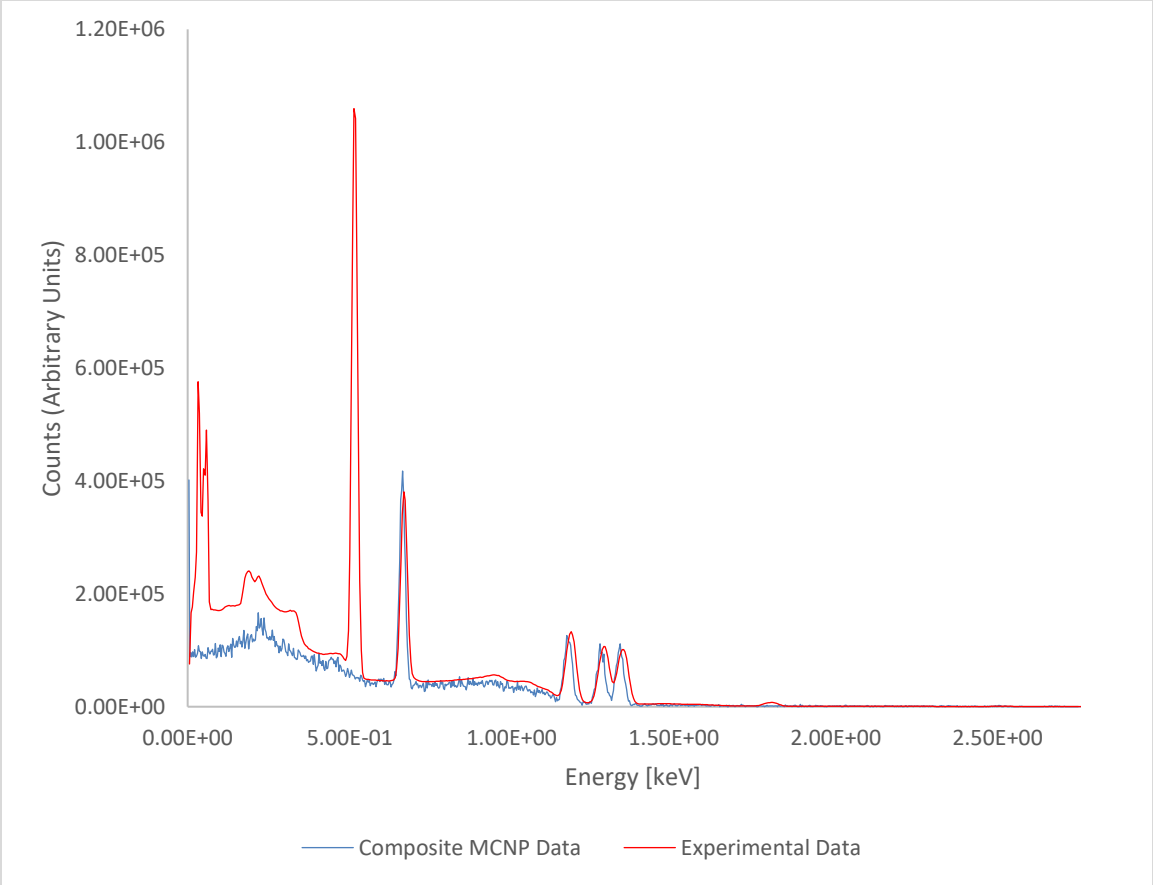

Figure 20: MCNP6 generated and experimentally collected normal single detector spectrum.

Seen in the normal spectra are the main gamma emissions from each of these sources: 661.7 keV from ^{137}Cs, 1173.2 keV and 1332.5 keV from ^{60}Co, and 1274.5 keV from ^{22}Na. However, the 511 keV emission from positron emission, subsequent annihilation, and Compton Continuum from ^{22}Na is only seen in the experimental data. This is because positrons were not tracked in the MCNP6 run. The MCNP6 simulation also lacked consideration of the intrinsic radioactivity of the $LaBr_3$:Ce crystal. This is most obvious at the slight discrepancy around 800 keV, and the missing x-rays at 35 keV.

The following figure shows the coincidence heatmap for the experimental measurements conducted in this comparison to MCNP6 simulations. Although coincidence performance was not investigated in MCNP6, the experimental coincidence heatmap is provided for reference.

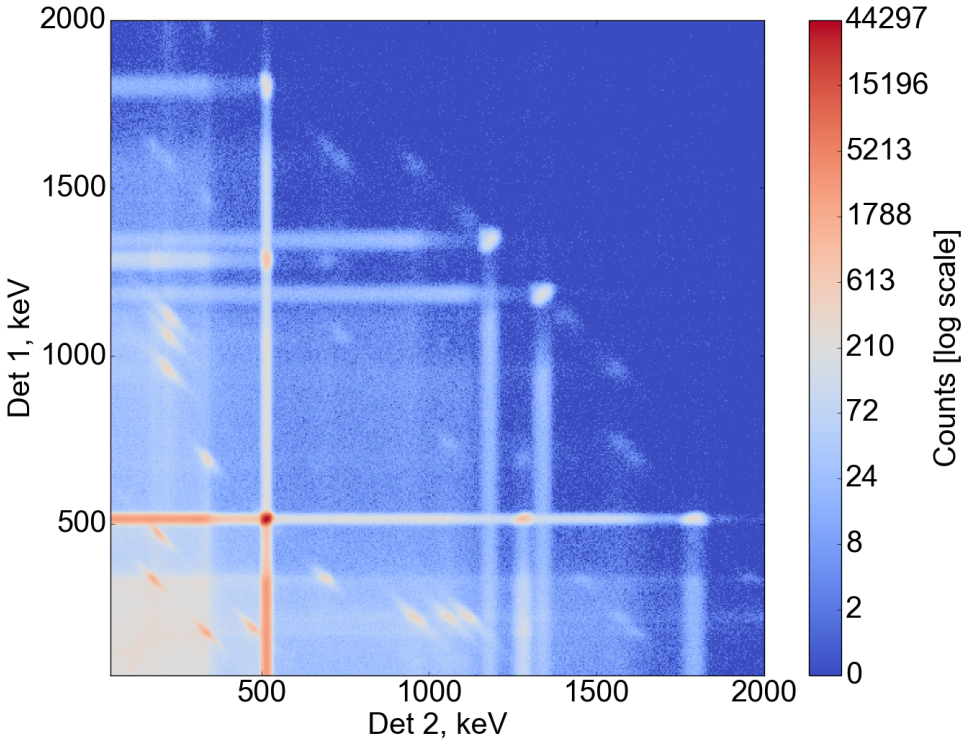

Figure 21: Experimental coincidence heatmap

Background Elimination via Coincidence Gating

The coincidence spectrum from a 20 hour background count with two $LaBr_3$:Ce detectors is shown in Figure 22 as a two-dimensional heatmap, with the energy bins of detectors 1 and 2 forming the y and x axes, respectively. A similar background count is also shown as a typical one dimensional gamma-ray spectrum for both single channel and coincident data in Figure 23.

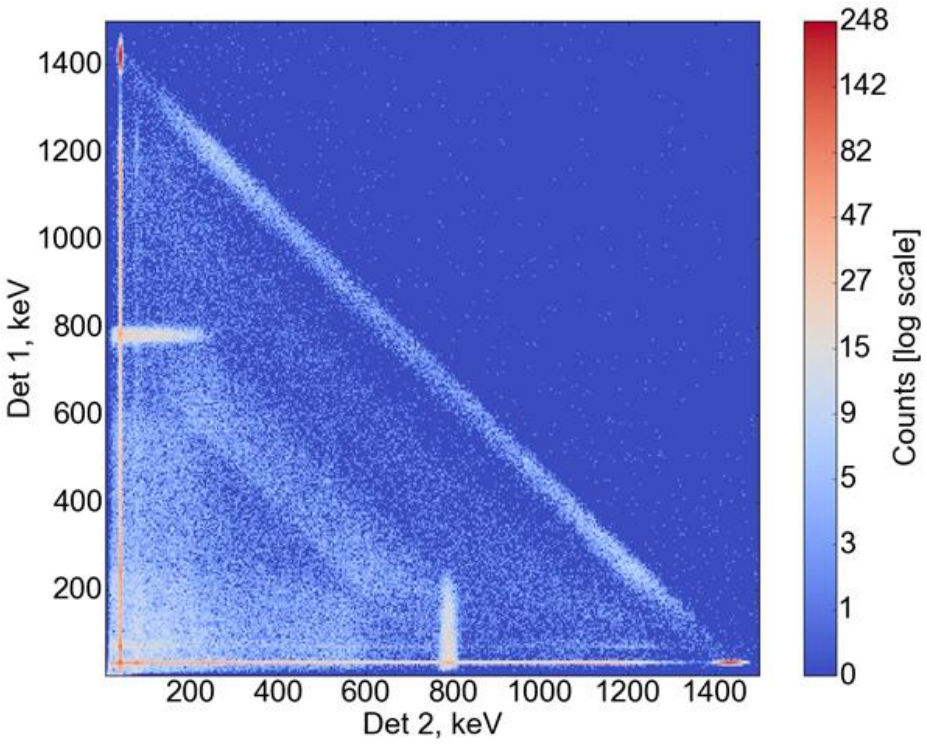

Figure 22: 20 hour coincident $LaBr_3$:Ce background count.

The peaks in this background spectrum include a 1435.8 keV photon, which is the result of ^{138}La decaying after electron capture to ^{138}Ba (66.4%), a 788.7 keV photon, which is the result of ^{138}La decaying by beta-emission to ^{138}Ce (33.6%), and a 35 keV ^{138}Ba x-ray, which is the result of the captured electron's shell being refilled.

First, the features of the two-dimensional coincidence heatmap will be discussed. Typically, the highest activity event in $LaBr_3$:Ce detector spectra is the 35 keV ^{138}Ba x-ray. This high activity x-ray manifests in the two-dimensional coincidence heatmap as a vertical line at detector 2's 35 keV point, and a horizontal line at detector 1's 35 keV point. These lines are coincidences of the 35 keV x-ray in one detector with Compton Scatters of the 1435.8 keV photon in the other detector. The next prominent feature is the smears that occur at 788 keV in one detector with low energies in the other detectors. This is a true coincidence of the intrinsic 788.7 keV photon of ^{138}La with its beta-emissions at an end point energy of 255 keV. The next largest background

event is the peak at 1435 keV, which has true coincidences and associated Compton Scattering coincidences with the 35 keV x-ray discussed previously. There is also a large diagonal streak in the coincidence heatmap connecting the two 1435 keV photons. Diagonal streaks such as this are typically 180 degree Compton Scattering events. This particular diagonal streak is the result of a 1435 keV photon depositing some of its energy in the detector in which it originated, and then Compton Scattering to the second detector and depositing the rest of its energy. Whenever diagonal Compton Scattering streaks are present in a coincidence heatmap, the sum of the coordinates of any point along that line will typically be a full energy peak that is seen in the spectrum. In this case, all points on the Compton Scattering streak have coordinates which sum to 1435, proving that they originate from ^{138}La decay to ^{138}Ba.

Many of these features can be seen, albeit with less detail, in the single channel spectra. The same background peaks are seen at 35 keV, 788 keV, and 1435 keV, however no coincidence information is present. Aside from the associated Compton continuums and other consequences of these peaks, the rest of the peaks of this spectrum are standard background peaks that would be present in the spectrum of any unshielded detector. A basic application of gamma-gamma coincidence involves gating over the entire range of this spectrum. By creating a gate 3000 keV wide, gamma rays only appear in the spectrum if they are coincident with any other gamma ray as shown in the lower curve in Figure 23.

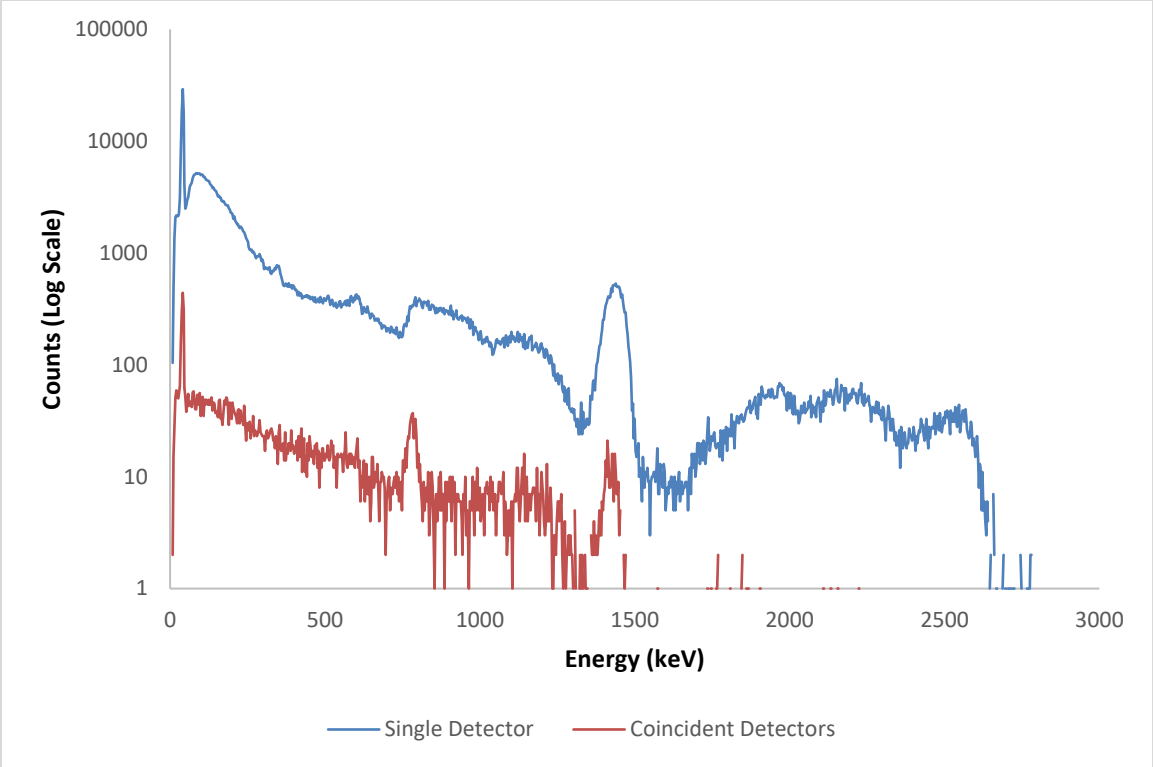

Figure 23: Background spectrum characteristic of $LaBr_3$:Ce detectors. The top curve is a single detector spectrum. The bottom curve is a coincidence spectrum with a spectrum-wide energy gate applied.

Upon applying this energy gate, the 1436 keV peak has been reduced by an order of magnitude. Counts across the entire spectrum have similarly been reduced by an order of magnitude or more. Full-energy coincidence gating causes a peak to appear at 788 keV, where there previously was no distinguishable peak. This is the result of the true coincidences between 788 keV photons and beta-emissions, which was evident in the two-dimensional heatmap earlier. Overall, coincidence gating results in a significant reduction in background, and provides additional clues as to the origin of various features of the spectrum. The background reduction associated with coincidence gating is particularly advantageous for $LaBr_3$:Ce detectors due to their strong intrinsic radioactivity. Similar energy gating methods can be utilized to de-convolute high activity spectra, as will be shown next.

SINGLE AND DUAL DETECTOR PEAK SIGNAL-TO-NOISE RATIO

Having established a proof-of-concept of coincidence methodologies for simplifying a background spectrum, the next stage in this experiment is to artificially create a complicated high activity spectrum to quantify the performance of each detector configuration as seen in Figure 24. SNR's of select gamma-ray peaks were measured with single and dual $LaBr_3$:Ce and HPGe detectors for a range of count rates. The 50 mCi ^{137}Cs source contains a shutter that can be adjusted to attenuate the gamma radiation to different levels. Changing this shutter position allowed input count rates of the experimental setup to vary from 20 to 400 kHz. The experimental setup is shown with the $LaBr_3$:Ce detectors below. An identical sample arrangement was made with HPGe detectors as well.

Figure 24: Experimental setup for SNR comparisons.

Three sample activity levels were measured (by varying the ^{137}Cs shutter position) with both detector types in single and dual detector configurations. The activity levels will be denoted "Low Count Rate" (LCR), "High Count Rate" (HCR), and "Very High Count Rate" (VHCR). Each data collection was performed for one hour. The following photopeak pairs from ^{152}Eu and

^{133}Ba were selected, and their SNR was measured for each count rate, detector type, and detector configuration. The gamma-ray pairs are shown in Table 1. The decay structures of ^{133}Ba and ^{152}Eu are provided for reference as well in Figure 25 and Figure 26, respectively. The decay structure of ^{133}Ba is much more manageable than that of ^{152}Eu. Almost every combination of gamma-ray energies in ^{133}Ba results in a coincidence event of appreciable magnitude, which makes it an excellent test source for coincidence experiments.

Table 1: A list of the coincident photopeaks selected for measurement.

Nuclide	Coincident Photopeak Energy Pairs [keV]
^{152}Eu	1: (121, 244), 2: (121, 444), 3: (121, 867), 4: (121, 965), 5: (121, 1112), 6: (121, 1408)
^{133}Ba	7: (80, 276), 8: (80, 303), 9: (80, 356)

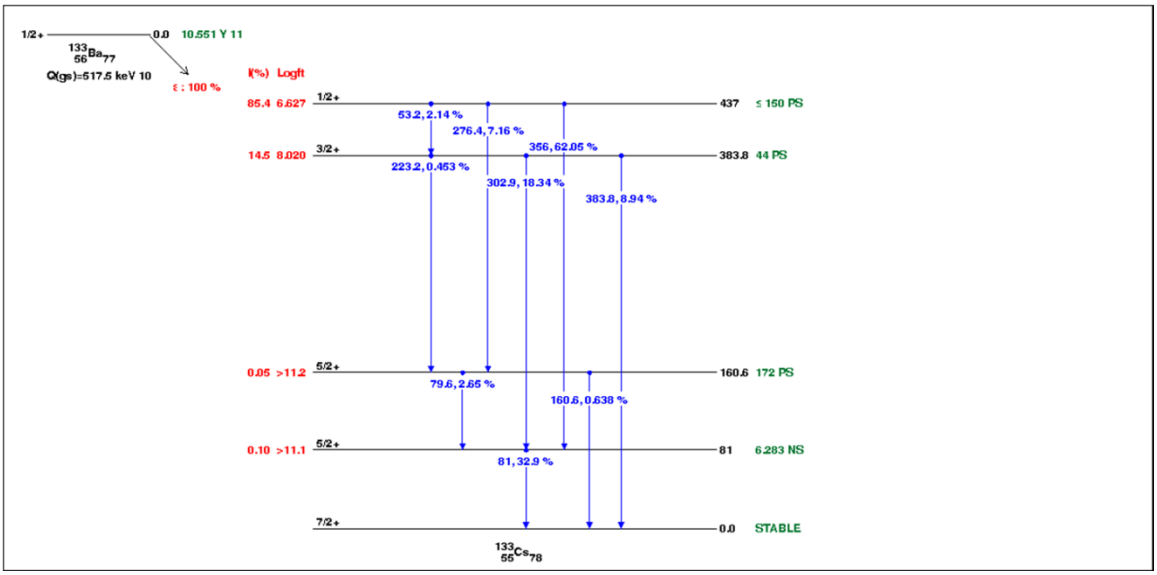

Figure 25: Decay structure of ^{133}Ba.

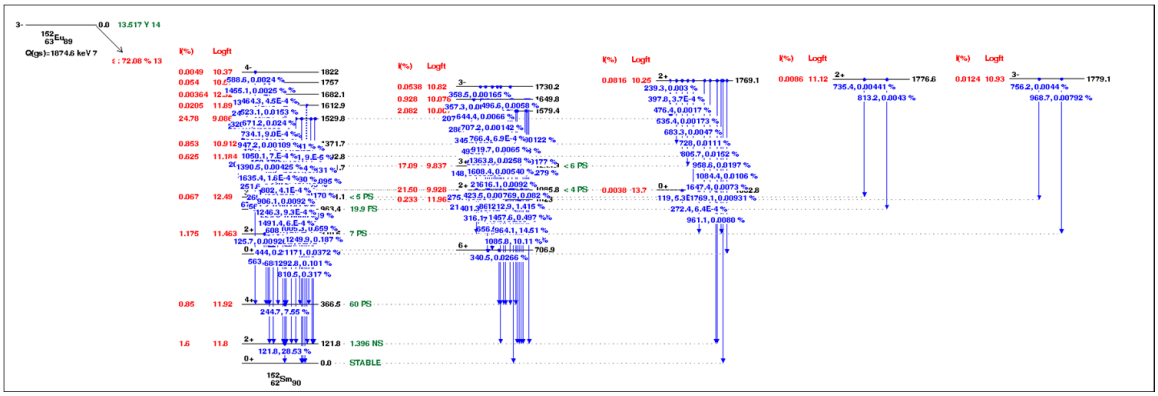

Figure 26: Decay structure of ^{152}Eu.

Results from this experiment include single channel and coincidence heatmaps from HPGe detectors and $LaBr_3$:Ce detectors for four sample activity levels. The one and two-dimensional data from each of these sample activity levels for both detector types are given below for reference.

Comparing the features of the single detector results for low count rate between HPGe and $LaBr_3$:Ce (Figs. 27 and 28 respectively), it is clear that the HPGe detectors were able to discriminate many more peaks than the $LaBr_3$:Ce detectors, which combined multiple peaks into multiplets throughout the spectrum. However, mapping the data onto a coincidence plane in Figure

29 significantly improves the discrimination capabilities of the $LaBr_3$:Ce detectors. Each coincident data point is well separated from the surrounding data, and the results between HPGe and $LaBr_3$:Ce detectors become comparable in terms of discrimination capabilities. Coincidence counting therefore has significant potential to alleviate the disadvantages associated with performing spectroscopy with scintillators, which have significantly worse energy resolution than semiconductors, by mapping results onto a two-dimensional plane.

The same general features of the low count rate data discussed above are also seen in the high count rate data (Figs. 30, 31, and 32). The single detector $LaBr_3$:Ce data is not particularly useful, however, mapping results onto a coincidence plane significantly improves peak discrimination capabilities. The primary difference in the high count rate data is the observed count rates between the two detector types. Compared to the low count rate data, the HPGe count rates have dropped by nearly an order of magnitude: max coincidence counts of 275 counts/bin in low count rate data, versus max coincidence counts of 30 counts/bin in high count rate data. This is due to the significant deadtime incurred by the HPGe detectors at this level of input count rate. On the other hand, the $LaBr_3$:Ce detectors have retained many more counts: max coincidence count rate of 5665 counts/bin in low count rate data versus 2106 counts/bin in high count rate data. As discussed earlier, the $LaBr_3$:Ce detectors have a significantly shorter pulse decay time, and therefore do not incur nearly as much deadtime when subject to significant input count rates.

The very high count rate scenario is where the strengths of the $LaBr_3$:Ce detectors are most obvious. The single detector results of Figure 31 are nearly completely dominated by the large ^{137}Cs peak. However, even while subject to input count rates on the order of 400 kHz, they are still able to extract a significant amount of useful data in the coincidence heatmap of Figure 32.

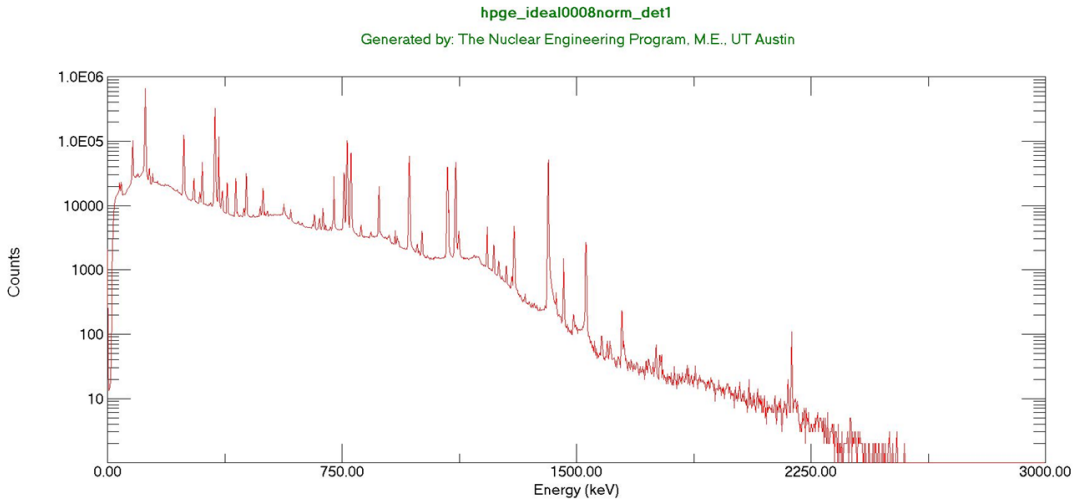

Figure 27: HPGe low count rate single detector results.

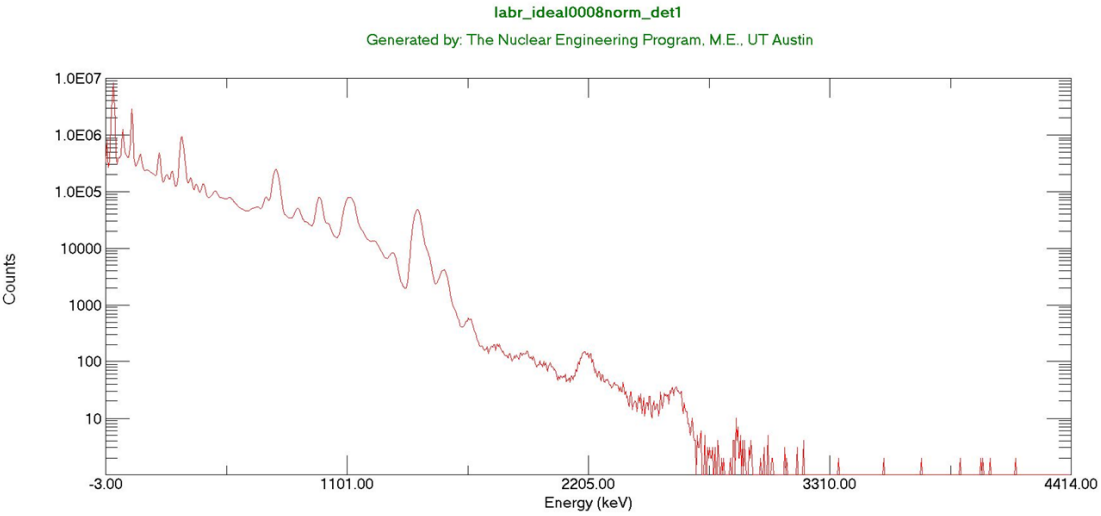

Figure 28: $LaBr_3$:Ce low count rate single detector results.

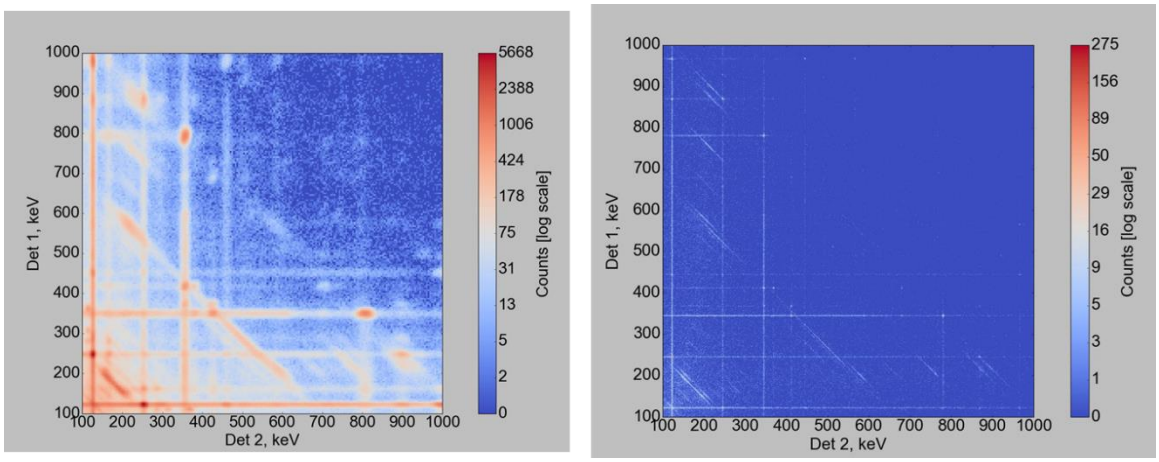

Figure 29: Left – $LaBr_3$:Ce coincidence heatmap for low count rate. Right – HPGe coincidence heatmap for low count rate.

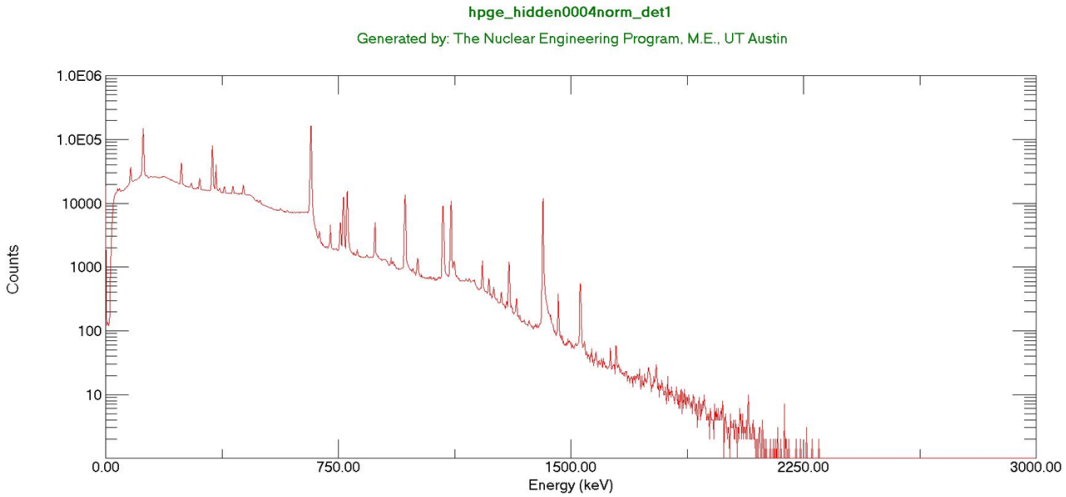

Figure 30: HPGe high count rate single detector results.

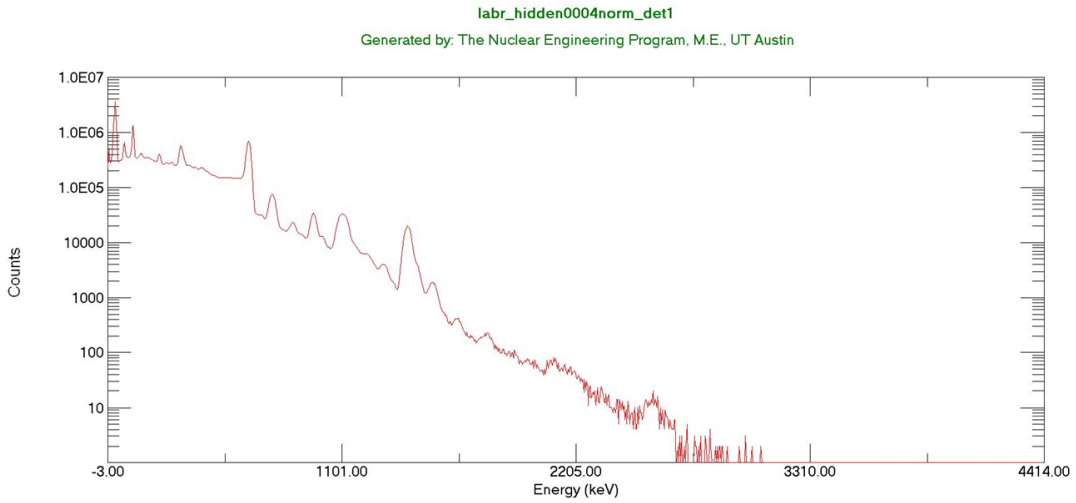

Figure 31: $LaBr_3$:Ce high count rate single detector results.

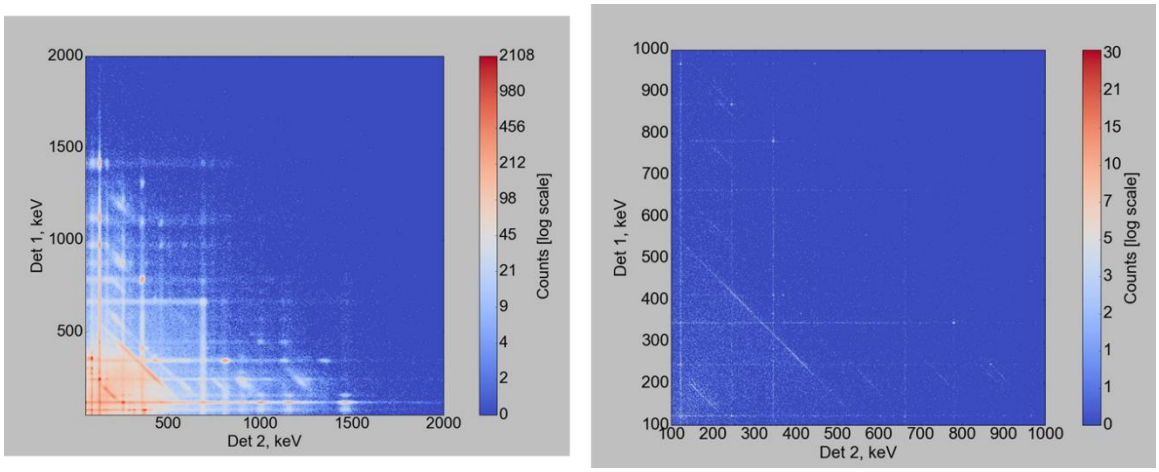

Figure 32: Left – $LaBr_3$:Ce coincidence heatmap for high count rate. Right – HPGe coincidence heatmap for high count rate. Note the different axes scales.

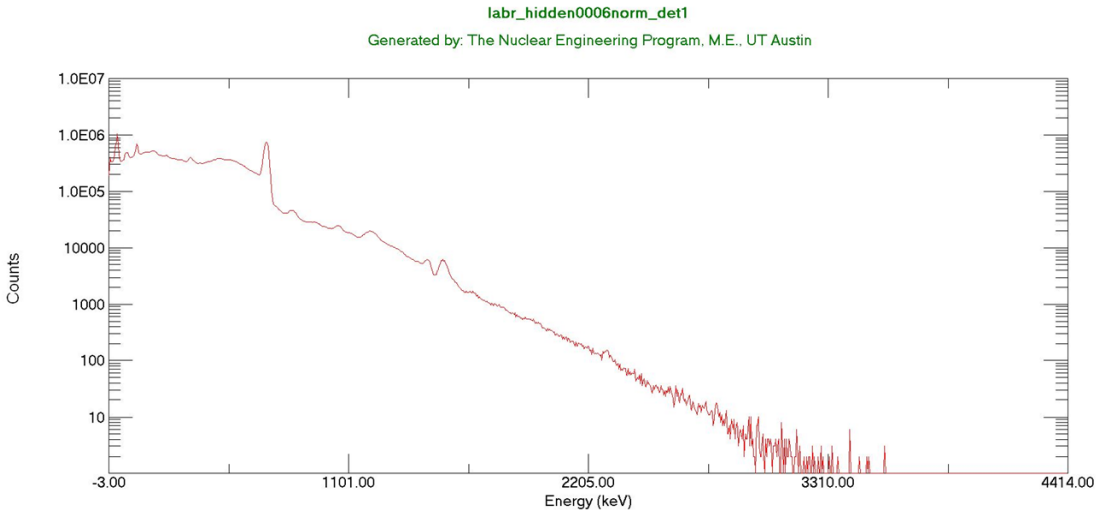

Figure 33: $LaBr_3$:Ce very high count rate single detector results.

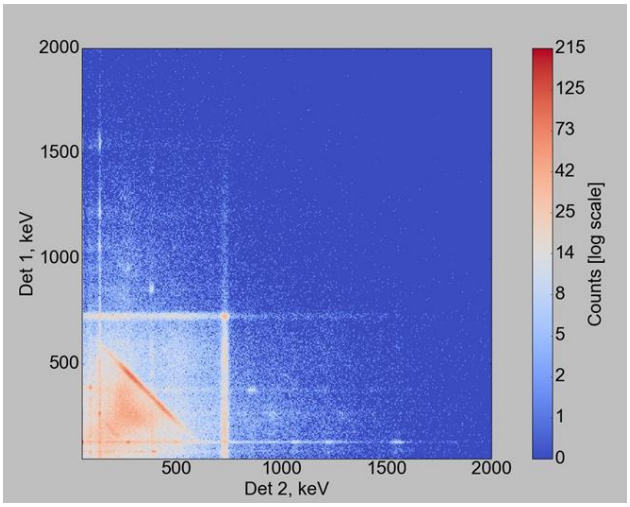

Figure 34: $LaBr_3$:Ce very high count rate coincidence heatmap results.

SNR's for the coincident photopeak energy pairs tabulated above were calculated for all of the single and dual detector measurements taken. SNR's were calculated by selecting each photopeak as a region of interest in the ORTEC Maestro software. The signal was defined as the gross area of each photopeak, and the noise was defined as the difference between gross and net areas of the photopeak. SNR was then calculated as the ratio of the defined signal and noise. Figures 35, 36, and 37 on the next few pages show the results of the SNR calculations. This data is also all summarized numerically in Table 2. Uncertainty bars are also shown for all SNR

calculations as one sigma. Note that the SNR improvements vary greatly between gamma-ray pairs. This is a result of the differing decay schemes between each coincidence pair. The capability of coincident measurements to improve SNR is highly dependent on the fractional intensity of the coincidence gamma-ray pair. For gamma-ray pairs that have much lower coincident intensities relative to their independent intensities, the improvement from employing coincidence measurements is reduced. In particular, gamma-ray pairs 5 and 6 have very low coincidence intensities relative to their independent intensities.

The results also show that, in general, the improvements obtained by employing coincidence measurements (versus single detector measurements) are greater in magnitude for higher count rates scenarios. The HCR improvements in SNR for both detector types are generally greater than the LCR improvements in SNR. The most dramatic evidence for this is in the VHCR case. Only $LaBr_3$:Ce detectors in coincidence were capable of detecting almost all of the gamma-rays. HPGe detectors at this activity level were fully paralyzed. These results suggest that performing measurements of spent nuclear fuel with coincident $LaBr_3$:Ce detectors will allow for identification of radionuclides that are unable to be detected with coincident HPGe detectors.

The next section will further investigate the capabilities of $LaBr_3$:Ce detectors for the potential application of fission product measurements on spent nuclear fuel by performing coincident spectroscopy on irradiated uranium samples of varying enrichment and identifying features of each spectrum.

Table 2: A tabulation of the SNR values and uncertainties for each photopeak measurement via each detection system.

	LCR				HCR				VHCR			
Gamma Pair	HPGe S	HPGe C	LaBr S	LaBr C	HPGe S	HPGe C	LaBr S	LaBr C	HPGe S	HPGe C	LaBr S	LaBr C
1	2.272±0.003	3.65±0.09	1.430±0.001	2.05±0.01	1.222±0.001	2.6±0.1	1.112±0.001	1.80±0.01	-	-	-	1.21±0.01
2	1.791±0.004	1.98±0.06	1.163±0.001	1.239±0.007	1.099±0.001	1.8±0.1	1.022±0.001	1.20±0.01	-	-	-	-
3	1.90±0.001	1.83±0.06	1.213±0.001	1.309±0.009	1.49±0.005	1.7±0.1	1.178±0.002	1.32±0.02	-	-	1.025±0.001	1.20±0.05
4	4.76±0.02	5.0±0.3	1.668±0.002	1.929±0.013	3.53±0.02	7±1	1.561±0.002	1.9±0.03	-	-	1.069±0.001	1.46±0.06
5	5.31±0.02	4.4±0.2	2.389±0.003	2.06±0.02	3.80±0.02	3.6±0.4	2.224±0.004	1.95±0.03	-	-	1.161±0.001	1.74±0.08
6	16.9±0.2	60±30	5.43±0.02	8.2±0.2	8.4±0.1	8±2	3.82±0.02	4.7±0.2	-	-	1.329±0.003	4.3±0.2
7	1.276±0.002	4.1±0.4	1.103±0.001	1.76±0.01	1.058±0.001	2.4±0.3	1.020±0.001	1.49±0.02	-	-	-	1.19±0.04
8	1.729±0.003	3.9±0.3	1.214±0.001	2.32±0.02	1.142±0.001	3.3±0.5	1.046±0.001	1.81±0.02	-	-	-	1.26±0.04
9	2.867±0.005	14±3	2.988±0.002	4.49±0.05	1.369±0.002	4.0±0.5	1.000±0.001	3.40±0.05	-	-	-	1.89±0.06

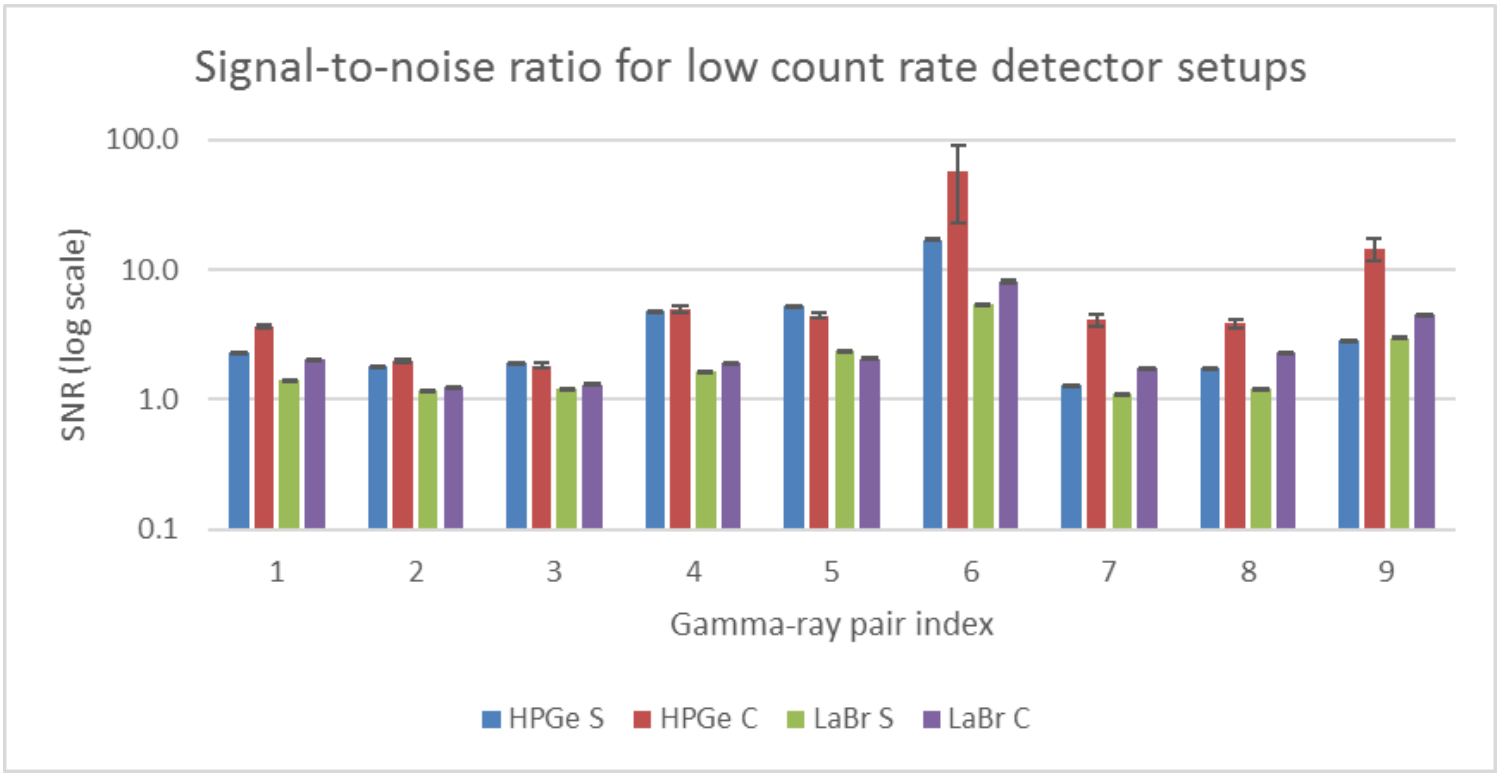

Figure 35: Signal-to-noise ratio values with uncertainty bars for low count rate measurements of each coincident photopeak pair with each detection system. The pair of coincident gamma-rays corresponding to each index are the pairs of gamma-rays listed in Table 1 in order. “S” stands for single and “C” stands for coincident.

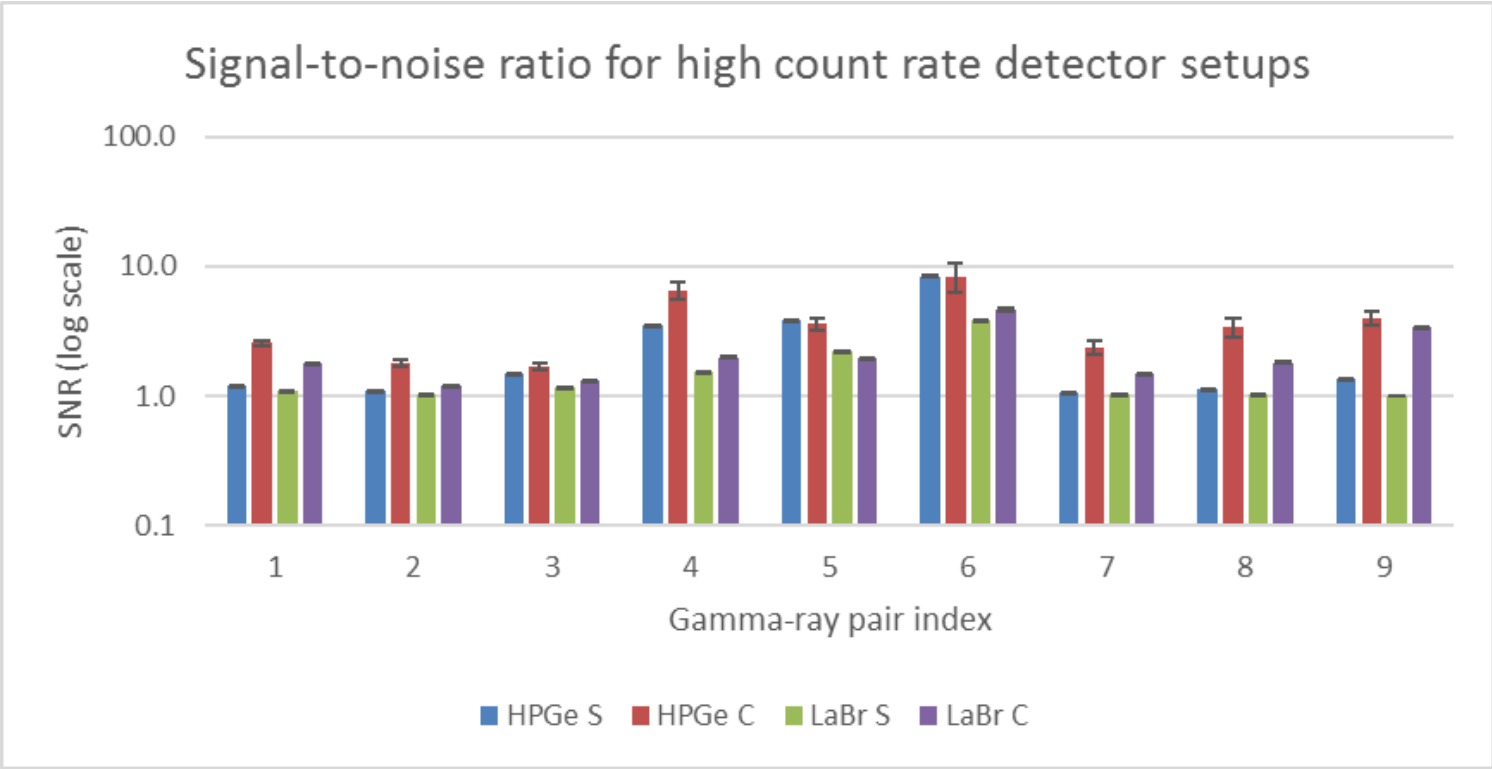

Figure 36: Signal-to-noise ratio values with uncertainty bars for high count rate measurements of each coincident photopeak pair with each detection system. The pair of coincident gamma-rays corresponding to each index are the pairs of gamma-rays listed in Table 1 in order. "S" stands for single and "C" stands for coincident.

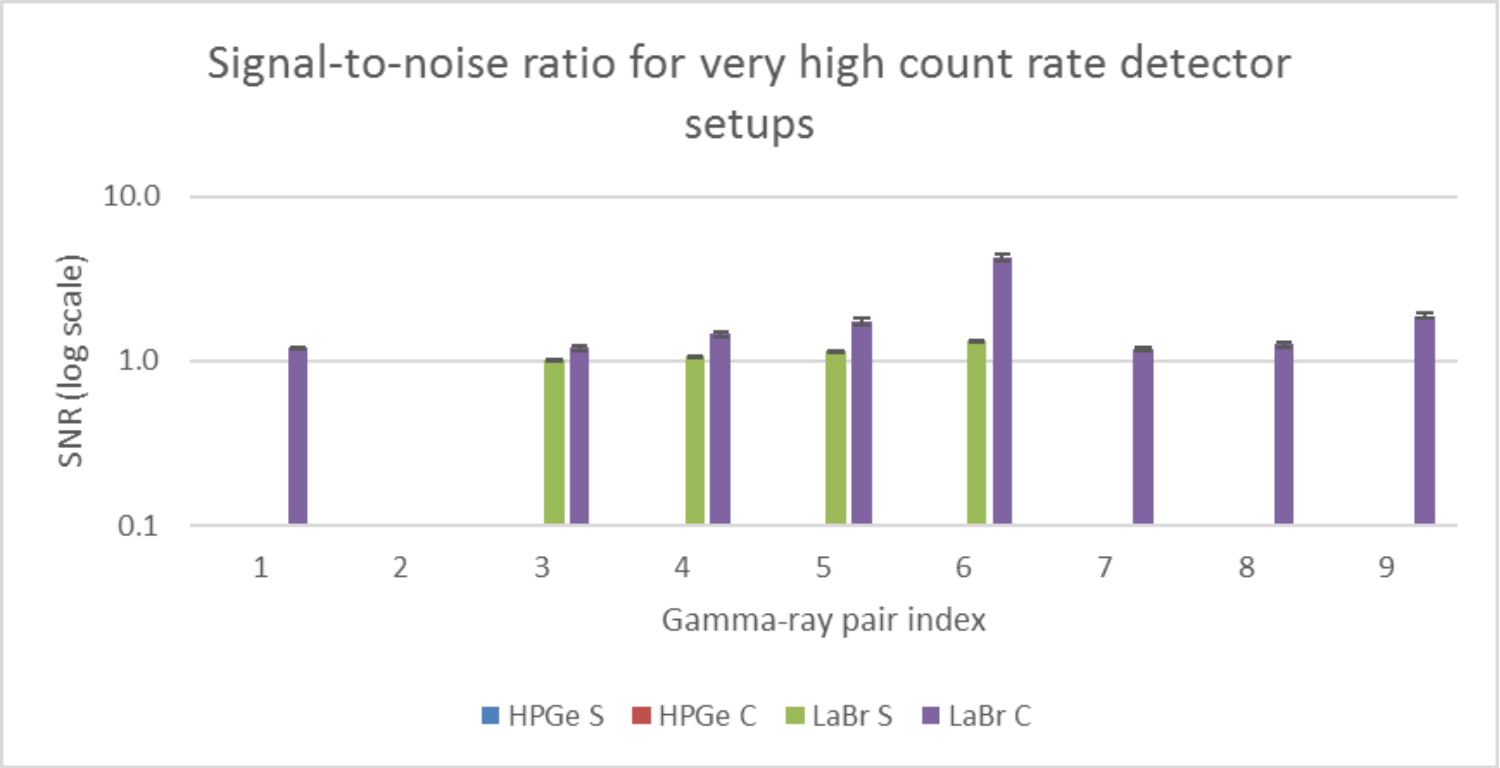

Figure 37: Signal-to-noise ratio values with uncertainty bars for very high count rate measurements of each coincident photopeak pair with each detection system. The pair of coincident gamma-rays corresponding to each index are the pairs of gamma-rays listed in Table 1 in order. “S” stands for single and “C” stands for coincident.

FISSION PRODUCT MEASUREMENTS

The results from the signal-to-noise ratio measurements in the previous section indicate that coincident $LaBr_3$:Ce detectors are most useful in high count-rate scenarios with complicated spectra. To further test the system in this type of scenario, coincident measurements with LaBr3:Ce detectors were conducted on irradiated uranium samples. This will serve as a useful analog to potential applications of such a detection system down the line for measurements of spent nuclear fuel for safeguards applications. The following sections will describe sample preparation, measurement conditions, and results.

Sample Preparation

Three 20 mg uranium samples were prepared from uranium certified reference material. Each sample was of a different enrichment: natural uranium (0.7%), low enriched uranium (3.0%), and high enriched uranium (63.0%). The three samples were encapsulated in quartz and irradiated in the TRIGA reactor at The University of Texas at Austin for one hour at a power level of 500 kW. This resulted in substantial sample activities. Therefore, the samples required cooling for several days before it was deemed safe to take them to the gamma spectroscopy lab.

The purpose of irradiation was to generate high activity fission products, which is a highly complicated and active spectrum: the conditions in which it was demonstrated that $LaBr_3$:Ce detectors excel. The capability of the system to extract useful information from a difficult measurement scenario such as this will then be investigated.

Measurement Conditions

Each uranium sample was measured via coincident $LaBr_3$:Ce detectors once every several days for a month following the irradiation. The resulting dataset is enormous and

multidimensional. There exists coincident heatmaps for uranium samples of three different enrichment levels, at twelve different times after irradiation over the course of a month. In total there are 35 coincident datasets (36 minus 1 lost spectrum). Extracting useful trends and quantitative results from this data is a formidable task. Additionally, several complications arose in measurement that contribute to the difficulty of this analysis. The resulting dataset will be presented in its entirety, qualitative trends will be discussed, the challenges and complications that resulted during these measurements will be discussed, and suggestions will be made for improving on such a measurement procedure in the future.

Results

The coincidence heatmaps for measurements of the three irradiated uranium samples are presented below. Each sample was measured for one hour twelve different times over the course of a month after irradiation. One HEU measurement conducted partway through the month was somehow lost, and that section of the figure is left blank. The features of the coincidence heatmaps will be discussed in terms of evolution over time, and the differences between the three enrichment levels will also be discussed. Table 3 lists the decay times post-irradiation associated with each of the twelve measurements for each of the three uranium samples.

Table 3: The elapsed time between irradiation and measurement for each of the one hour long measurements.

Measurement	1	2	3	4	5	6	7	8	9	10	11	12
Decay time [days]	4	6	8	11	13	15	18	20	22	25	27	29

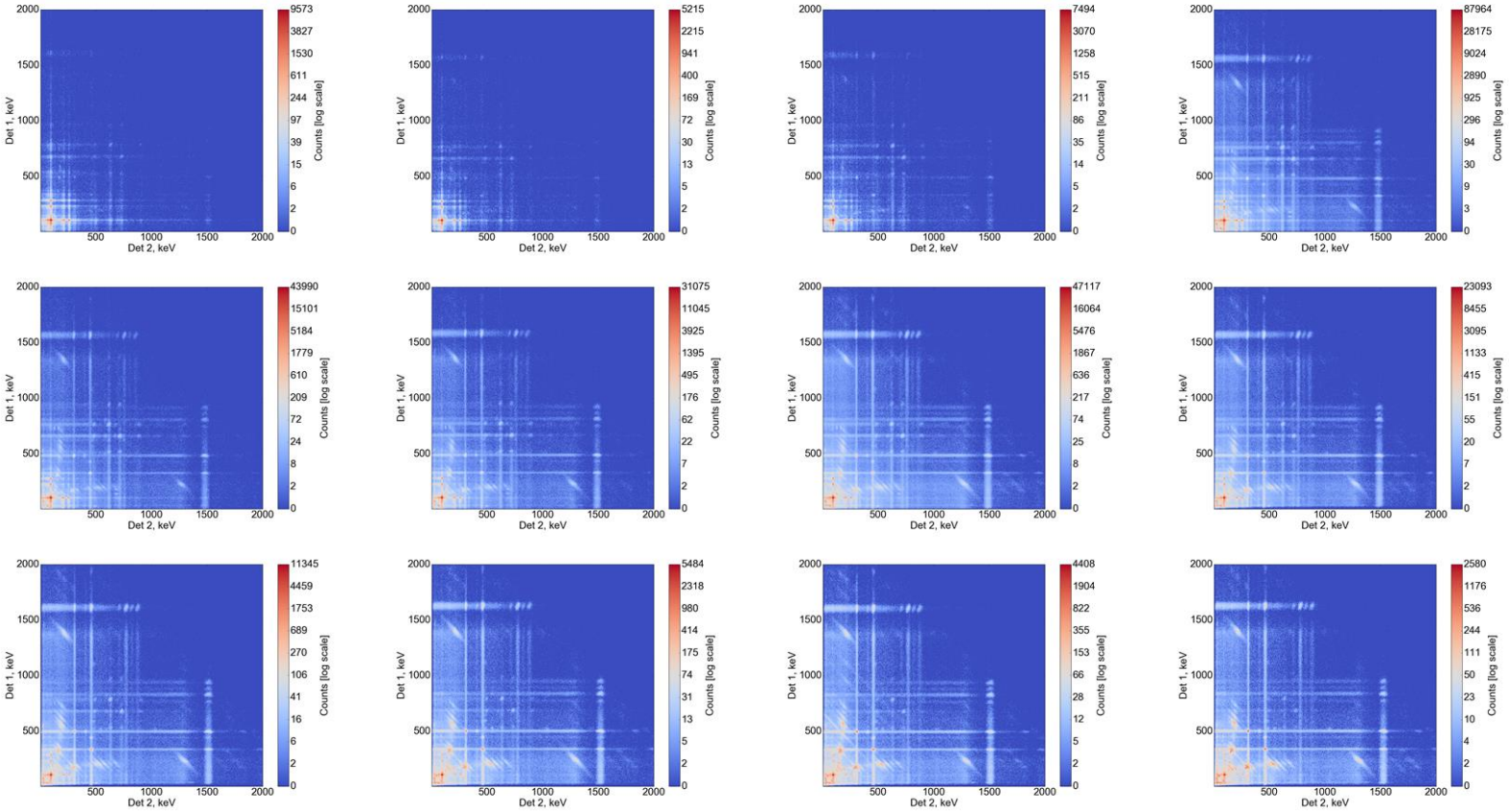

Figure 38: Irradiated natural uranium (0.7% ^{235}U) coincident heatmaps representing one hour data collections every few days over the course of a month post-irradiation.

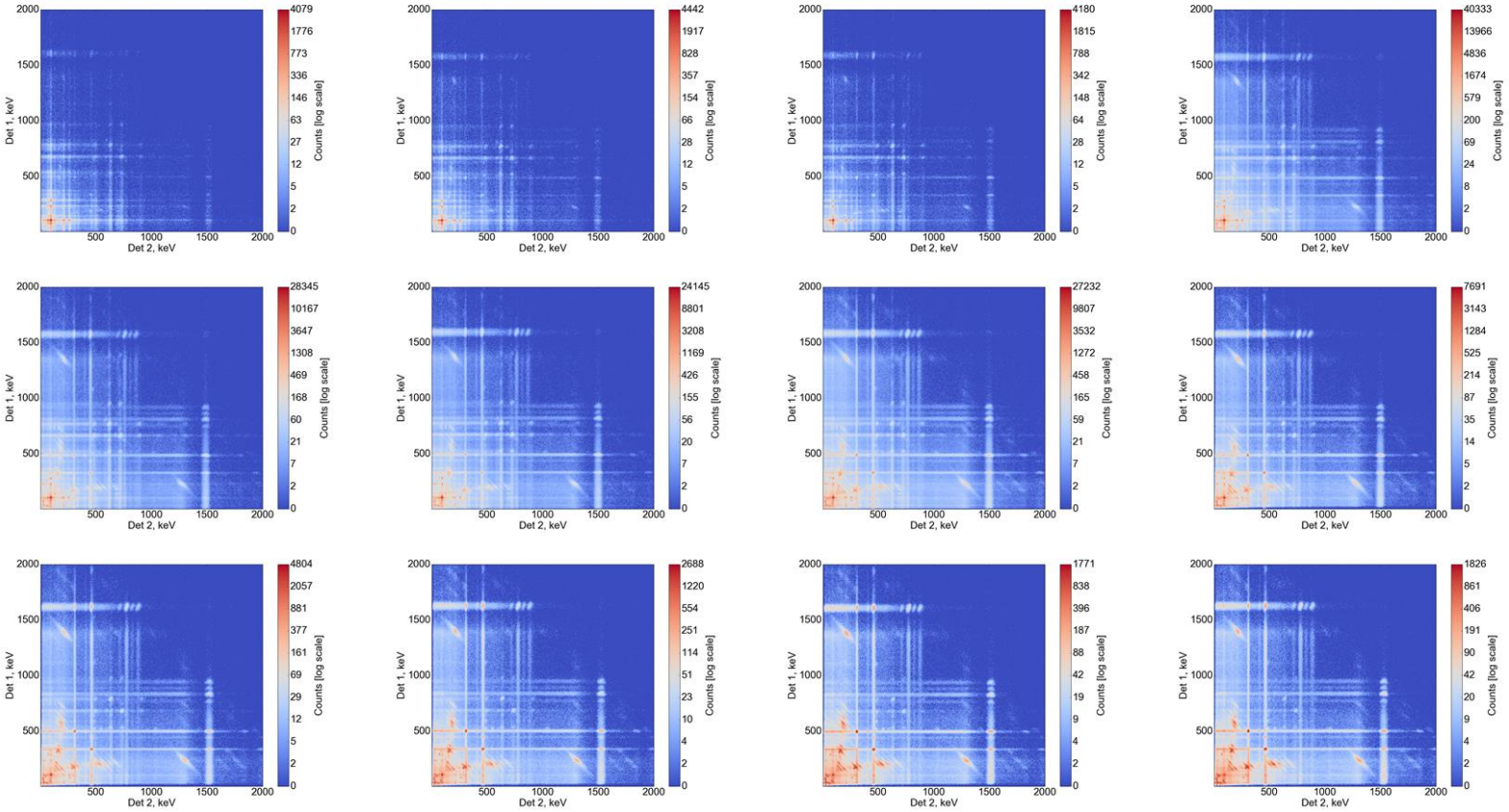

Figure 39: Irradiated low enriched uranium (3.0% ^{235}U) coincident heatmaps representing one hour data collections every few days over the course of a month post-irradiation

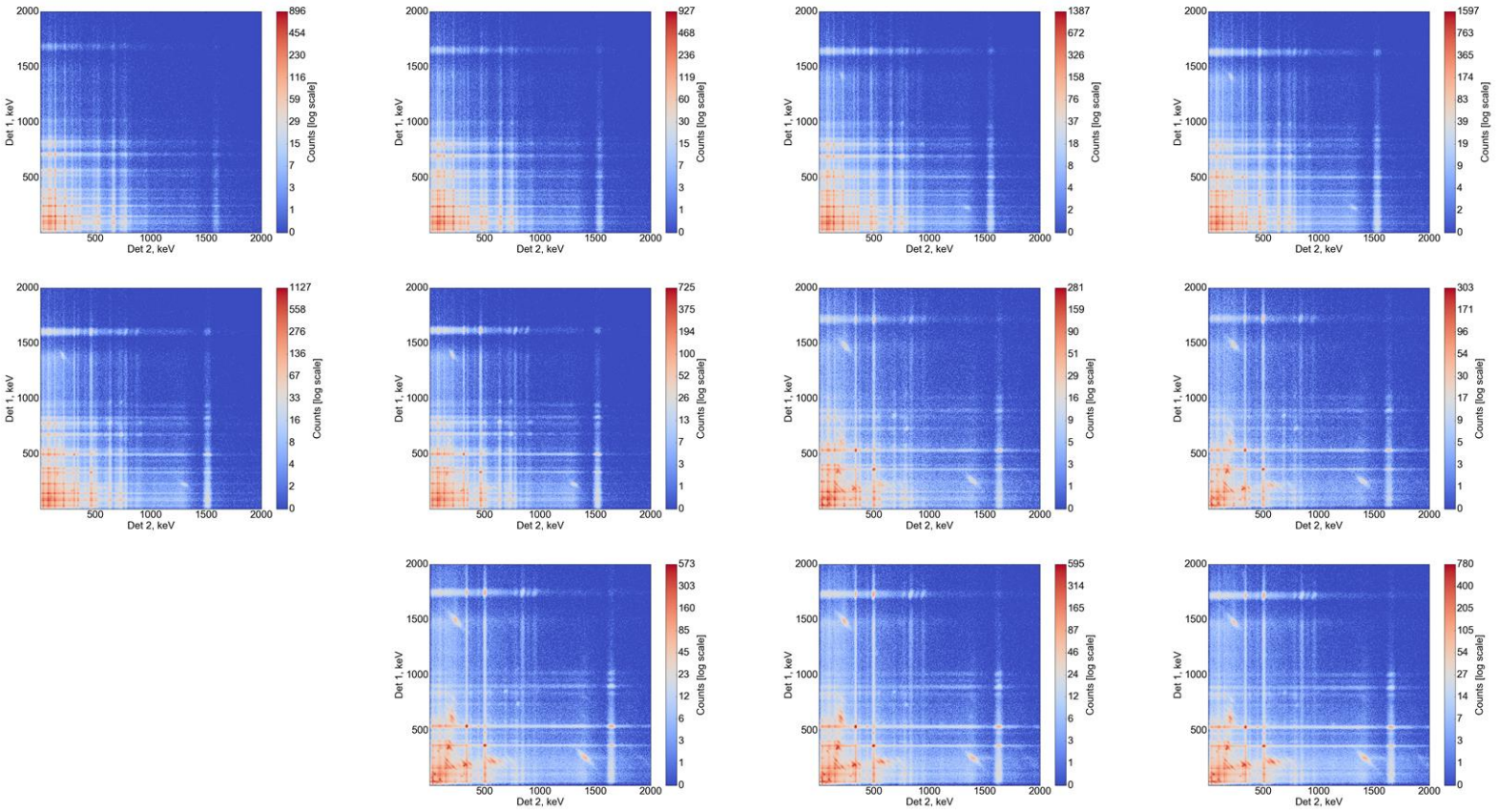

Figure 40: Irradiated high enriched uranium (63.0% ^{235}U) coincident heatmaps representing one hour data collections every few days over the course of a month post-irradiation.

There are a large number of features of the sizable datasets shown in Figures 38, 39, and 40 to discuss. For instance, observing the first coincidence dataset corresponding to each of the uranium enrichment levels, it appears that the highest count rates were observed in the natural uranium, followed by the LEU, and with the HEU having the lowest count rate. This is due to deadtime effects in the detectors. In actuality, the HEU had by far the highest activity levels, and created significant deadtimes in the $LaBr_3$:Ce detectors. This resulted in the need to make compromises in other aspects of coincident performance. In particular, the distance between the detectors was increased during early measurement periods in order to avoid complete detector deadtime. Even with the 16 cm inter-detector distance employed for the first few measurements, the input rates to the detectors were on the order of 30 kHz for natural and LEU, and 300 kHz for HEU. Unfortunately, increasing the inter-detector distance has a negative effect on the efficiency of coincidence measurements on the order of r^{-4} that outpaces the decrease in count rate on the order of r^{-2} achieved by increasing inter-detector distance. This increased inter-detector distance was preserved until the samples reached significantly lower count rates about two weeks into the data collection. From this point forward, all measurements were conducted with 2.54cm of distance between the two detectors. This ability to decrease inter-detector distance towards the end of the measurement period improves the quality of the latter measurements for each uranium sample considerably.

Another complication that was observed during these measurements was inconsistency with the energy calibration of the system. There were considerable shifts in the energy calibration of the system during all measurements. However, the shift was strongest during HEU measurements. It is suspected that the energy calibration of the $LaBr_3$:Ce detectors is dependent upon the count rate measured by the system. For HEU

measurements, gain shifts close to +100 keV in the spectrum could be observed. The inconsistency of energy calibration is present in most of these datasets, and therefore represents a significant challenge when attempting to identify particular radionuclide signatures throughout the spectrum. Without a reliable correction method for this inconsistency in the energy calibration, it is difficult to determine fission product contents with full confidence. Thankfully, the nature of coincidence data provides multi-dimensional radionuclide fingerprints, which helps to offset some of the uncertainty associated with the drifting energy calibration.

Identified Fission Products

Based on measurements of the most prominent coincident photopeak pairs, the fission products listed in the table below were successfully identified in some of the datasets. Many of the coincident gamma-ray pairs present in the heatmaps were not identified. This is due to the laborious nature of searching the nuclear data for coincident gamma-ray information, which is coupled with the uncertainty arising from the poor energy calibration resulting from high count rates.

It should be noted that the fission products listed in Table 4 represent the best guesses of the author as to the source of each coincidence point present in the heatmaps, especially when considering the substantial uncertainties in the energy calibration for most datasets. This work should be considered a scoping study of the feasibility of identifying fission products in a complicated and high activity spectrum with a portable scintillation coincidence system such as $LaBr_3$:Ce detectors. Validation could be performed with smaller, lower activity samples with a coincident HPGe detection system with much more stable energy calibration.

Table 4: A tabulation of fission products whose coincidence signatures appear in the presented measurement data.

Fission Product	Identified Coincidence Pairs [keV]	Halflife
^{150}Eu	(334, 439)	36.9 y
^{98}Tc	(652, 745)	$4.2*10^6$ y
^{149}Gd	(150, 299)	9.3 d
^{94}Nb	(703, 871)	$2.03*10^4$ y
^{150}Eu	(402, 439)	36.9 y
^{105}Ag	(306, 155)	41.3 d
^{156}Tb	(262, 111), (212, 111)	5.35 d
^{134}Cs	(795, 605)	2.1 y

Chapter 6: Conclusion

SUMMARY OF RESULTS

This thesis has set out to characterize the performance of an $LaBr_3$:Ce detection system in a coincidence configuration. The coincidence timing window, energy resolution, efficiency, and signal-to-noise ratio in representative counting situations have been quantified. In order to put the characterization results into context, comparisons have been made to: single detector configurations, alternative coincidence detector configurations, and Monte Carlo simulations. A more difficult measurement representative of high activity spent nuclear fuel has also been conducted on irradiated uranium samples of varying enrichment.

A procedure has been presented for the accurate determination of the optimum coincidence timing window by measurements of true and random coincidence pairs from ^{60}Co while varying the timing window. This procedure has shown that $LaBr_3$:Ce detectors can handle much smaller timing windows than HPGe detectors, and benefit from timing windows much smaller than what can be achieved with a Pixie-4's 13.3 ns timing resolution.

Oscilloscope measurement comparisons between the $LaBr_3$:Ce and HPGe detectors have demonstrated and verified the faster response of the $LaBr_3$:Ce detectors, and provided evidence for their capability to handle much higher count rates with lower dead-times than HPGE detectors.

Efficiency and energy resolution comparisons have been made between the two detector types. The HPGe detector was superior in this regard. However, $LaBr_3$:Ce detectors represent a significant step in bridging the energy resolution gap between scintillators and semiconductors. Furthermore, comparisons to MCNP6 simulations have

verified the efficiency of the $LaBr_3$:Ce detectors at high energies, but had discrepancies at lower energies which were discussed.

Preliminary MCNP6 simulations of a single $LaBr_3$:Ce detector measuring an array of point sources was performed and compared to experimental results. The experimental and simulation results showed strong agreement on the detector response. However, the self-background of the detector and the positron interactions resulting from ^{22}Na were missing from the MCNP simulation.

The self-background resulting from intrinsic radioactivity in the $LaBr_3$:Ce detectors have been measured and discussed. It has been shown that employing gamma-gamma coincidence measurements significantly reduces this self-background, alleviating one of the primary concerns associated with using $LaBr_3$:Ce detectors.

Experimental measurements of a complicated assortment of coincident gamma-rays have been performed with single and coincident systems consisting of HPGe and $LaBr_3$:Ce detectors. The performance of each of the four detection systems has been quantified by calculating the signal-to-noise ratio for each measured photopeak. The data show that coincidence configurations result in substantial SNR improvements over single detector configurations for gamma-rays that characteristically decay in coincidence with high intensity relative to their independent decay intensities. These data demonstrate that, for complicated that exist in coincidence it is of great benefit to exploit gamma-gamma coincidence counting.

At lower count rates, HPGe detectors have superior SNR to $LaBr_3$:Ce detectors. However, in very high count rate regimes, HPGe detectors are unable to perform. There are no data for VHCR HPGe detectors because this activity level fully paralyzed the detectors. The maximum count rate that was successfully measured with HPGe detectors

was about 150 kHz. By comparison, $LaBr_3$:Ce detectors successfully measured data at over 400 kHz. This demonstrates that, for very high count rate scenarios, only $LaBr_3$:Ce detectors are sufficient. For safeguards analysis, such as in situ measurements of spent nuclear fuel, $LaBr_3$:Ce detectors are therefore an excellent option. Their portability, ability to handle extreme count rates, and excellent timing performance make them ideal for gamma-gamma coincidence measurements of very high activity samples such as spent nuclear fuel.

Finally, measurements of irradiated uranium samples ranging from naturally enriched to highly enriched uranium were conducted to determine the presence of coincident photon-emitting fission products in each of the samples. One hour measurements of all three uranium samples were conducted every few days over the course of a month. The time evolution of the coincident heatmaps of each enrichment level were presented and discussed. The signatures of a few fission products which characteristically decay with coincident photon emissions were identified within the coincident heatmaps. The challenges associated with these measurements were discussed. Primarily, high sample activity causes gain shifts within the detectors which alter the energy calibration of the system, making precise energy identification more difficult, particularly when measuring an array of sources that each have highly different activity levels.

The ability to handle extreme count rates is of particular importance in coincidence counting. In single detector counting, moving the source further away from the detector reduces the count rate, and makes activity levels a non-issue. However, for coincidence counting, it is critical that the two detectors are as close to each other, and as close to the sample, as possible. This is because the efficiency of coincidence counting drops off as x^{-4}, where x is the source-detector distance. Count rate drops only as x^{-2}. There is no benefit

to moving coincidence detectors further away from the measured source, so long as the dead time is less than 100%. $LaBr_3$:Ce detectors therefore have the potential to fulfill the unique role of extending the capabilities of gamma-gamma coincidence spectroscopy to extreme count rate regimes on the order of 400 kHz or greater, which could have substantial impact on analysis of spent nuclear fuel for safeguard purposes.

FUTURE WORK

This work presented a well-characterized radiation detection system consisting of two cerium-doped lanthanum bromide detectors in a gamma-gamma coincidence configuration. The strengths, weaknesses, and best applications of such a system have been presented, with benchmarks to existing and well-studied systems. This will lay the ground work for similar systems to be developed and applied to real-world measurements in the future.

Further Applications

In particular, it has been demonstrated that coincident $LaBr_3$:Ce detectors excel in measurements of high count-rate gamma emitting samples, particularly when the gamma-ray signatures are complex and contain many radionuclides. Nuclear safeguards measurements of spent nuclear fuel is a challenging measurement situation that could greatly benefit from the use of such a detection system. Although irradiated uranium reference materials serve as a useful experimental source of fission products for measurement, the next logical step would be to measure actual spent nuclear fuel with such a system to determine its usefulness in real-world applications.

Unresolved Challenges

This work has also identified several of the challenges of using such a coincidence system. Future investigations aimed at improving existing radiation detection systems could select a few of these challenges and develop solutions which will ultimately improve the capabilities of such coincidence systems further.

In particular, high count-rate measurements have an impact on the energy calibration of the $LaBr_3$:Ce detectors. It would be useful to perform a detailed investigation of the mechanisms behind this energy calibration offset, and derive relations that describe its dependence on the input count rate. This would allow for the energy calibration shifts to be automatically corrected for in post-processing if there is a clear dependence on count rate, as is currently predicted.

Although the optimum timing window for coincidence gating was determined experimentally in this work, no investigation was done to study the timing offset between the two detectors. It is possible that, if such a timing offset exists, and could be corrected for, further refinements to the coincidence timing window could be developed. Additionally, it is shown that narrower timing windows than could be achieved with the currently employed Pixie-4 module will further improve the system. For example, the coincidence timing window could be further constrained by utilizing an XIA Pixie-500, which will further improve the performance and signal-to-noise ratio achievable with coincident detection. The XIA Pixie-500 has a timing resolution of 2 ns vs the utilized XIA Pixie-4 with a 13.3 ns timing resolution. The measured trend of $LaBr_3$:Ce coincidence performance versus timing window suggests that this will result in a substantial improvement in rejection of random coincidence events.

Additional Investigations

MCNP simulations were performed to compare the performance of a single $LaBr_3$:Ce detector to expected results. There exists an extension to MCNP called Polimi, which adds nuclear decay structure information to the sampling of radionuclide decay. This makes it possible to perform accurate simulations of gamma-gamma coincidence measurements. It would be useful to compare the performance of the real-world experimental $LaBr_3$:Ce coincidence system to MCNP coincidence simulation results to determine the system's capability to be improved through further refinement of various settings, etc.

MCNP simulations with Polimi would also be useful to determine the theoretical coincidence heatmaps resulting from irradiation of uranium samples of varying enrichments. Analysis of the coincidence heatmaps is difficult due to the large number of coincidence signatures contained within it. MCNP Polimi simulations could therefore be used to determine the contributing radionuclides to each feature within the coincidence heatmap.

Appendix

MCNP6 Code: Efficiency Determination

```
c
c*************************** File Description ****************************
c
c This file will be used to determine the efficiency of a single LaBr3:Ce
c detector.
c
c Description:
c A photon-emitting point source is created 10 cm from the face of the
c detector. The point source emits 10 different photons with energies that
c match those emitted by experimentally-used monoenergetic sources. An F8
c tally on the detector cell measures the resulting spectrum. A GEB card
c alters the spectrum with an energy resolution function that matches what is
c experimentally observed in LaBr3:Ce detectors. 1E7 particles are simulated.
c Energy bins collect the pulses. The efficiency is calculated as the net
c area of the photopeak in each energy bin corresponding to an intial photon
c energy divided by the expected number of emissions at that energy.
c
c Author: Adam Drescher
c  2017/03/24
c
c *** Cell Cards ***
c
1 1 -5.06 -1            IMP:P=1 IMP:E=1   $ LaBr3:Ce Detector
2 2 -.001205 -2#(-1:-3) IMP:P=1 IMP:E=1   $ Problem boundary
3 0 2                   IMP:P=0 IMP:E=0   $ Problem outer bound
4 3 -2.375 1 -3         IMP:P=1 IMP:E=1   $ Aluminum Housing

c *** Surface Cards ***
c
1 RCC  -3.81  0 0    3.81 0 0  1.905      $ LaBr crystal
3 RCC  -3.91  0 0    3.91 0 0  1.955      $ Aluminum Housing
2 RPP -4 11  -2 2  -2 2                   $ Problem bound

c *** Data Cards ***
c
c  ----- Materials
c
M1 57000 .2375 35000 .7125 58000 .05      $ LaBr3:Ce (5% cerium)
M3 13000 1                                $ Aluminum
M2 6000 .000150 7000 .784431 8000 .210748 18000 .004671
c                                         $ PNNL Air Standard
c
c  ----- Physics Options
c
MODE P E
PHYS:P
```

```
c
NPS 1E7
c
c  ----- Desc. of Source
c
SDEF pos=10 0 0 erg=d1
ACT DG=LINES THRESH=0 NONFISS=ALL        $ photons emitted at discrete energies
c with no intensity threshold
SI1 L .060 .088 .16586 .279 .393 .66164
      .834827 1.115 1.1732 1.3325
SP1 D 1 1 1 1 1 1 1 1 1
c
c
c  ----- Cell Tally Cards
c
F8:p 1                                   $ Detector Pulse Height Tally
E8 0 128i 1.5                            $ Detector energy bins
```

MCNP6 CODE: SOURCE COLLECTION SIMULATION

```
c
c*************************** File Description ******************************
c
c This file will be used to simulate the response of an LaBr3:Ce detector when
c measuring a set of gamma-emitting source standards.
c
c Description:
c Measurements of a collection of gamma-emitting sources including Na-22,
c Cs-137, and Co-60 are conducted utilizing one lanthanum bromide detector.
c The results are output in a single detector spectrum with energy bins and
c appropriate GEB energy resolution broadening. The deck is run once for each
c of the three sources. The resulting spectra from each of the three sources
c are post-processed by weighting to match the activities of the experimentally
c measured sources, which allows the simulated spectrum to match the
c experimental data as closely as possible. The inclusion of the second
c detector is to match the experimental geometry, however no measurements are
c conducted with the second detector.
c
c Author: Adam Drescher
c  2017/03/24
c
c *** Cell Cards ***
c
1 1 -5.06 -1 IMP:P=1 IMP:E=1                $ Left Detector
2 1 -5.06 -2 IMP:P=1 IMP:E=1                $ Right Detector
3 2 -19.1 -3 IMP:P=1 IMP:E=1                $ Sample
4 0 -4#(-1:-3:-2) IMP:P=1 IMP:E=1           $ Problem boundary
5 0 4  IMP:P=0  IMP:E=0                     $ Problem outer bound

c *** Surface Cards ***
c
1 RCC -4.1 0 0   3.8 0 0  1.9               $ Left Detector
2 RCC  0.3 0 0   3.8 0 0  1.9               $ Right Detector
3 RCC 0 -3.2 0  0 6.4 0  0.3                $ Sample of Na22, Cs137, and Co60
4 RPP -4.2 4.2  -4 4  -2 2                  $ Problem bound

c *** Data Cards ***
c
c  ----- Materials
c
M1 57000 .2375 35000 .7125 58000 .05        $ LaBr3:Ce (5% cerium)
M2 11022 1                                  $ Sample of Na22
c 27060 1  11022 1 55137 1
c  ----- Physics Options
```

```
c
MODE P E F
PHYS:P
c
NPS 1E5
c
c  ----- Desc. of Source
c
SDEF x=d1 y=d2 z=d3 par=d4 cel=3 TME=d5
ACT DG=LINES THRESH=0 NONFISS=ALL              $ Photons emitted at discrete
energies
c with no intensity threshold
SI1 -0.3 0.3
SP1 0 1
SI2 -3.2 3.2
SP2 0 1
SI3 -0.3 0.3
SP3 0 1
SI4 L SP
SP4 w -3
SP5 -7 5.565e16
c
c
c  ----- Cell Tally Cards
c
F8:p 1                                        $ Detector Pulse Height Tally
FT8 GEB .001 .0205 .3
E8 0 1e-6 1e-3 1022i 3                        $ Detector energy bins
```

References

Abbas, K., Morel, J., Etcheverry, M., & Nicolaou, G. (1998). Use of miniature CdZnTe X/gamma detector in nuclear safeguards: Characterisation of spent nuclear fuel and uranium enrichment determination. *Nuclear Instruments and Methods in Physics Research, Section A: Accelerators, Spectrometers, Detectors and Associated Equipment*, *405*(1), 153–158. https://doi.org/10.1016/S0168-9002(97)01143-1

Alharbi, T., Mason, P. J. R., Regan, P. H., Podolyák, Z., Mărginean, N., Nakhostin, M., … Ghugre, S. S. (2012). Gamma-ray fast-timing coincidence measurements from the $^{18}O+^{18}O$ fusion-evaporation reaction using a mixed $LaBr_3$-HPGe array. *Applied Radiation and Isotopes : Including Data, Instrumentation and Methods for Use in Agriculture, Industry and Medicine*, *70*(7), 1337–9. https://doi.org/10.1016/j.apradiso.2011.11.040

Barton, J. C., & Michaelis, E. G. (1960). Multiple Geiger Counter Coincidences due to Gamma Radiation.

Beausang, C. W., & Simpson, J. (1996). Large arrays of escape suppressed spectrometers for nuclear structure experiments. *Journal of Physics G: Nuclear and Particle Physics*, *22*, 527. https://doi.org/10.1088/0954-3899/22/5/003

Bender, S., Heidrich, B., & Ünlü, K. (2015). Compton suppressed $LaBr_3$ detection system for use in nondestructive spent fuel assay. *Nuclear Instruments and Methods in Physics Research, Section A: Accelerators, Spectrometers, Detectors and Associated Equipment*, *784*, 474–481. https://doi.org/10.1016/j.nima.2014.12.025

Bramlitt, E. T. (1966). Gamma-Gamma Coincidence Counting Applied to Chlorine Analysis by Neutron Activation, *38*(12), 1669–1674.

Britton, R., Jackson, M. J., & Davies, A. V. (2015). Quantifying radionuclide signatures from a gamma-gamma coincidence system. *Journal of Environmental Radioactivity*, *149*, 158–163. https://doi.org/10.1016/j.jenvrad.2015.07.025

Ciupek, K., Jednoróg, S., Fujak, M., & Szewczak, K. (2014). Evaluation of efficiency for in situ gamma spectrometer based upon cerium-doped lanthanum bromide detector dedicated for environmental radiation monitoring. *Journal of Radioanalytical and Nuclear Chemistry*, *299*(3), 1345–1350. https://doi.org/10.1007/s10967-013-2906-z

Erikson, L., Keillor, M., Aalseth, C., Hossbach, T., Mizouni, L., Stavenger, T., … Rutherford, C. (2013). Determining HPGe total detection efficiency using c-c coincidence. *Journal of Radioanalytical and Nuclear Chemistry*, *296*(2), 705–710. https://doi.org/10.1007/s10967-012-2186-z

Gilmore, G. (2008). *Practical Gamma-ray Spectrometry 2nd Edition*. *Training*. https://doi.org/10.1002/9780470861981

Gunnink, R., Colby, L. J. J., & Cobble, J. W. (1959). Absolute Beta Standardization Using 4 Pi Beta-Gamma Coincidence Techniques, (2), 796–798.

Hofstadter, R., & Mcintyre, J. A. (1950). Measurement of Gamma-Ray Energies with Two Crystals in Coincidence, 819–825.

Horne, S., & Landsberger, S. (2011). Selenium and mercury determination in biological samples using gamma–gamma coincidence and Compton suppression. *Journal of Radioanalytical and Nuclear Chemistry*, *291*(1), 49–53. https://doi.org/10.1007/s10967-011-1268-7

Iltis, A., Mayhugh, M. R., Menge, P., Rozsa, C. M., Selles, O., & Solovyev, V. (2006). Lanthanum halide scintillators: Properties and applications. *Nuclear Instruments and Methods in Physics Research, Section A: Accelerators, Spectrometers, Detectors and Associated Equipment*, *563*(2), 359–363. https://doi.org/10.1016/j.nima.2006.02.192

Kajrys, G., Irshad, M., Landsberger, S., Lecomte, R., Paradis, P., & Monaro, S. (1982). High spin states and band structure in ^{97}Tc. Physical Review C.

Kajrys, G., Landsberger, S., Lecomte, R., Paradis, P., & Monaro, S. (1982). Level structure of ^{97}Tc investigated via the ^{97}Mo(p,nγ) reaction. Physical Review C.

Khang, P. D., Hai, N. X., Tan, V. H., & Dien, N. N. (2011). Gamma-gamma coincidence spectrometer setup for neutron activation analysis and nuclear structure studies. *Nuclear Instruments and Methods in Physics Research, Section A: Accelerators, Spectrometers, Detectors and Associated Equipment*, *634*(1), 47–51. https://doi.org/10.1016/j.nima.2011.01.025

Kim, J. I., Speecke, A., & Hoste, J. (1965). Neutron Activation Analysis of Copper in Bismuth by Gamma-Gamma Coincidence Measurement, *33*.

Knoll, G. F. (2010). *Radiation Detection and Measurement*. John Wiley.

Konki, J., Greenlees, P. T., Jakobsson, U., Jones, P., Julin, R., Juutinen, S., … Uusitalo, J. (2012). Comparison of gamma-ray coincidence and low-background gamma-ray singles spectrometry. *Applied Radiation and Isotopes*, *70*(2), 392–396. https://doi.org/10.1016/j.apradiso.2011.10.004

Löher, B., Savran, D., Fiori, E., Miklavec, M., Pietralla, N., & Vencelj, M. (2012). High count rate spectroscopy with LaBr3:Ce scintillation detectors. *Nuclear Instruments and Methods in Physics Research Section A: Accelerators, Spectrometers, Detectors and Associated Equipment*, *686*, 1–6. https://doi.org/10.1016/j.nima.2012.05.051

Markovic, N., Roos, P., & Nielsen, S. P. (2016). Digital gamma-gamma coincidence HPGe system for environmental analysis. *Applied Radiation and Isotopes*, (December). https://doi.org/10.1016/j.apradiso.2016.12.017

McGrath, C. A., Garrett, P. E., Villani, M. F., & Yates, S. W. (1999). Gamma-gamma coincidence measurements following inelastic neutron scattering. *Nuclear Instruments and Methods in Physics Research, Section A: Accelerators, Spectrometers, Detectors and Associated Equipment*, *421*(3), 458–463. https://doi.org/10.1016/S0168-9002(98)01170-X

Metwally, W. A., Gardner, R. P., & Sood, A. (2007). Using gamma-gamma coincidence measurements to validate Monte Carlo generated detector response functions. *Nuclear Instruments and Methods in Physics Research, Section B: Beam Interactions with Materials and Atoms*, *263*(1 SPEC. ISS.), 50–53. https://doi.org/10.1016/j.nimb.2007.04.137

Milbrath, B. D., Choate, B. J., Fast, J. E., Hensley, W. K., Kouzes, R. T., & Schweppe, J. E. (2007). Comparison of $LaBr_3$:Ce and NaI(Tl) scintillators for radio-isotope identification devices. *Nuclear Instruments and Methods in Physics Research Section A: Accelerators, Spectrometers, Detectors and Associated Equipment*, *572*(2), 774–784. https://doi.org/10.1016/j.nima.2006.12.003

Mora, M. V., Padilla, A. G., Palomino, J. L. C., & Terremoto, L. A. A. (2011). Nondestructive burnup measurements by gamma-ray spectroscopy on spent fuel elements of the RP-10 research reactor. *Progress in Nuclear Energy*, *53*(4), 344–353. https://doi.org/10.1016/j.pnucene.2011.01.003

Navarro, J., Ring, T. A., & Nigg, D. W. (2014). Gamma-ray simulated spectrum deconvolution of a $LaBr_3$ 1- x 1- in. scintillator for nondestructive ATR fuel burnup on-site predictions.

Oshima, M., Toh, Y., Hatsukawa, Y., Koizumi, M., Kimura, A., Haraga, A., … Sushida, K. (2008). Multiple gamma-ray detection method and its application to nuclear chemistry. *Journal of Radioanalytical and Nuclear Chemistry*, *278*(2), 257–262. https://doi.org/10.1007/s10967-008-0303-9

Pagden, I. M. H., & Sutherland, J. C. (1970). Resolving Power of Gamma Ray Coincidence Spectrometry Using Lithium Drifted Germanium Detectors and Its Application to Multiple Radioisotope Analysis, *42*(3), 383–387.

Piero, a., Bacchi, M. a., & Fernandes, E. a. N. (2008). INAA with gamma-gamma coincidence for selenium determination in food. *Journal of Radioanalytical and Nuclear Chemistry*, *278*(3), 761–765. https://doi.org/10.1007/s10967-008-1607-5

Schmitz-feuerhake, I. (1970). Studies on Three-dimensional Scintigraphy with Y-y-Coincidences, *15*(4), 649–656. https://doi.org/10.1088/0031-9155/15/4/004

Saint Gobain. (2009). Scintillation Products Technical Note.

Tomlin, B. E., Zeisler, R., & Lindstrom, R. M. (2008). Gamma-Gamma Coincidence Spectrometer for Instrumental Neutron-Activation Analysis. *Nuclear Instruments*

and Methods in Physics Research, Section A: Accelerators, Spectrometers, Detectors and Associated Equipment, *589*(2), 243–249. https://doi.org/10.1016/j.nima.2008.02.094

Vaccaro, S., Tobin, S. J., Favalli, A., Grogan, B., Jansson, P., Liljenfeldt, H., … Vo, D. (2016). PWR and BWR spent fuel assembly gamma spectra measurements. *Nuclear Instruments and Methods in Physics Research, Section A: Accelerators, Spectrometers, Detectors and Associated Equipment*, *833*, 208–225. https://doi.org/10.1016/j.nima.2016.07.032

Willman, C., Håkansson, A., Osifo, O., Bäcklin, A., & Svärd, S. J. (2006). Nondestructive assay of spent nuclear fuel with gamma-ray spectroscopy. *Annals of Nuclear Energy*, *33*(5), 427–438. https://doi.org/10.1016/j.anucene.2005.12.005

XIA LLC. (2013). User's Manual Digital Gamma Finder (DGF) Pixie-4, (May). Retrieved from http://www.xia.com/Manuals/Pixie4_UserManual.pdf

Xiang, Q., Tian, D., Hao, F., Chu, C., Ding, G., Zeng, J., & Luo, F. (2013). Self-calibration method for cerium-doped lanthanum bromide scintillator detector in the 0.1–2.0 MeV energy range. *Journal of Radioanalytical and Nuclear Chemistry*, *299*(3), 1439–1445. https://doi.org/10.1007/s10967-013-2782-6

Yoho, M., & Landsberger, S. (2015). Erratum to: Determination of selenium in coal fly ash via γ–γ coincidence neutron activation analysis. *Journal of Radioanalytical and Nuclear Chemistry*. https://doi.org/10.1007/s10967-015-4253-8

Zhang, W., Ungar, K., Stukel, M., & Mekarski, P. (2014). A gamma-gamma coincidence/anticoincidence spectrometer for low-level cosmogenic $^{22}Na/^{7}Be$ activity ratio measurement. *Journal of Environmental Radioactivity*, *130*, 1–6. https://doi.org/10.1016/j.jenvrad.2013.12.018

Zhang, W., Yi, J., Mekarski, P., Ungar, K., Hauck, B., & Kramer, G. H. (2011). A gamma-gamma coincidence spectrometric method for rapid characterization of uranium isotopic fingerprints. *Journal of Radioanalytical and Nuclear Chemistry*, *288*(1), 43–47. https://doi.org/10.1007/s10967-010-0868-y

Vita

Adam Drescher completed high school in New Hampshire in 2012. He then attended The University of Texas at Austin, and graduated with a bachelor's degree in Physics in 2015. He continued his education at The University of Texas at Austin, and graduated with a master's degree in Nuclear and Radiation Engineering in 2017. He will continue his education at The University of Texas at Austin with the intent of obtaining a Ph. D. in Nuclear and Radiation Engineering.

Permanent email address: awdrescher@gmail.com

This thesis was typed by the author.